Article

Mathematical models for FDG kinetics in cancer: a review

Sara Sommariva [1], Giacomo Caviglia [2], Gianmario Sambuceti [3] and Michele Piana [4,*]

[1] LISCOMP, Dipartimento di Matematica, Università di Genova, Genova, Italy; sommariva@dima.unige.it
[2] Dipartimento di Matematica, Università di Genova, Genova, Italy; caviglia@dima.unige.it
[3] Dipartimento di Scienze della Salute, Università di Genova and Ospedale Policlinico San Martino IRCCS Genova, Genova, Italy;
[4] LISCOMP, Dipartimento di Matematica, Università di Genova, Genova, Italy and CNR - SPIN Genova, Genova, Italy. piana@dima.unige.it
* Correspondence: piana@dima.unige.it

Abstract: Compartmental analysis is the mathematical framework for the modelling of tracer kinetics in dynamical Positron Emission Tomography. This paper provides a review of how compartmental models are constructed and numerically optimized. Specific focus is given on the identifiability and sensitivity issues and on the impact of complex physiological conditions on the mathematical properties of the models.

Keywords: Positron Emission Tomography (PET); FDG; tracer kinetics; compartmental analysis.

1. Introduction

Glucose plays a crucial and for a large part unexplained role in cancer metabolism [46]. Indeed, a common feature of tumor pathological metabolism is an increased glucose uptake, together with its fermentation to lactate, even under aerobic conditions [26]. This behavior is known as Warburg effect [53] and the revealing of its mechanism and function is one of the most intriguing open issues of cancer biochemistry since almost one hundred years.

2-deoxy-2-[18F]fluoro-D-glucose (FDG) [34] is a glucose analog that is systematically utilized as a radioactive tracer in nuclear medicine. In fact, once injected in a living organism, FDG is carried to tissues by blood, is diffused in tissues, is transported into cells by the same transporters (GLUTs) as glucose and is eventually trapped into cells after phosphorylation by hexokinase (HK). Further, Warburg effects increase the FDG consumption by cancer cells, which makes this tracer useful for cancer detection and staging, and for the assessment of clinical therapies.

FDG Positron Emission Tomography (FDG-PET) [38] is a functional imaging modality that utilizes FDG as a tracer in order to quantitative assess FDG metabolism in tumors (but other pathologies are systematically investigated as well by means of this imaging technique). FDG-PET measures the radiation emitted by the tracer injected in the organism and these measurements encode, in a very indirect way, two kinds of information: the localization of FDG accumulation in the body and the rate with which FDG changes its metabolic status along time. In order to decode such sophisticated information, two inverse problems must be solved:

1. **Image reconstruction inverse problem** [33]: to reconstruct the spatio-temporal distribution of FDG inside the tissue by solving the integral equation that connects the FDG densito to the measured radiation by means of the Radon transform.
2. **Compartmental inverse problem** [54]: to model the tracer kinetics by solving the non-linear time-dependent equation that connects the tracer coefficients to the reconstructed FDG concentration.

The focus of the present review is on the compartmental inverse problem. In this framework, on the one hand the recorded tissue activity corresponds to the superposition of

the tracer signal in the blood, in the interstitial tissue, and within the cell. On the other hand, the unknowns are the parameters associated to the kinetics of the tracer, which mimics the kinetics of glucose. From a mathematical perspective, compartmental models rely on the law of concentration conservation between functionally homogeneous conditions; this leads to a Cauchy problem whose number of ordinary differential equations corresponds to the number of compartments. In this Cauchy problem the constant coefficients provide the rate of tracer flow between compartments and, since they are able to describe the action of the enzymes metabolizing the tracer, they represent the unknowns of the compartmental problem. At a more specific level, typical technical assumptions are that:

- Only one compartment is allowed to exchange tracer with the environment.
- The input function, i.e. the tracer concentration introduced into the tissue by the blood, is known by means of either experimental measurements or mathematical modeling.
- The overall tracer concentration associated to the organ of interest (typically, the tumor) is known as a function of time.
- Both the linearity of fluxes between compartments and vanishing initial conditions hold.
- The kinetic coefficients are constant and homogeneous in the tissue.

Within this framework, the present review will consider just basic schemes with a limited number of variables. For them, we will provide a description of the input data (Section 2) and of how the compartmental models can be constructed (Section 3). A specific focus will be given to standard graphical approaches and to the connection between them and the more general compartmental analysis (Section 4). Further, we will discuss the consequences of the intrinsic ill-posedness of compartmental problems, including their lack of uniqueness and of sensitivity (Section 5). We will also illustrate some specific compartmental models that are related to as much specific physiological conditions (Section 6). And we will briefly review some of the optimization methods that have been formulated and implemented in order to reduce such models (Section 7). Our conclusions will be offered in Section 8.

2. The experimental data in the compartmental game

The metabolic pattern of most solid tumors shows an increased glucose consumption, even under aerobic conditions [51]. The mechanisms underlying this Warburg effect remain largely elusive, but a number of studies documented a direct relationship between glucose consumption and aggressiveness in cancer tissues. Although direct measurement of the continuous flux of glucose molecules through lesion-populating cells is extremely difficult, a reliable estimate was made possible by the peculiar kinetic features of the radioactive glucose analogue 2-[18F]-2deoxy-D-glucose (FDG). Indeed, FDG is transported through cell membranes by the same GLUT transporters as glucose, and it is trapped into the cytosol by phosphorylation catalyzed by the same hexokinases. However, differently from glucose-6-phosphate (G6P), FDG6P is a false substrate for downstream enzymes channeling G6P to glycolysis or the pentose-phosphate pathway. Thus, FDG6P accumulates in cells and tissues, and its amount is considered an accurate marker of their overall glucose consumption [6,28,32]. Accordingly, the measured tracer content may be employed in non invasive cancer detection and staging, and in the assessment of drug treatments.

In vivo, cancer FDG retention is dependent upon blood glucose level [44,56], drugs [11], and overall tracer availability in blood, which in turn depends on the amount of administered activity and the diffusion process throughout the whole body, after injection. Tracer concentration in blood also varies with time as a consequence of physiological factors, related to urinary elimination [11], accumulation in liver [12], absorption by brain [47], and the different accumulation rates of the various tissues [3].

Positron emission tomography (PET) measures the radiation emitted by the target tissue in vivo, following an intravenous administration of tracer molecules. The measuring device is calibrated so that the activity distribution inside the tissue is reconstructed. The output may vary from the estimate of the concentration of activity in a subregion of the

tissue at a chosen instant, to the time course of the activity in a given time interval, where the independent time variable t [min] measures the time interval from the tracer infusion.

In this section we recall a few essential features of the sources of data providing the input for kinetic models of tracer dynamics. We consider first the standardized uptake value (SUV), which approximates the tracer metabolic assessment by using a single time frame (static imaging); next we consider (dynamic) estimates of the time course of tracer concentration in blood (input function) and tracer concentration in the target tissue, which are both obtained from a time series of images.

2.1. Standardized Uptake Value

Perhaps, the standardized uptake value (SUV) is the simplest parameter which is used to quantify tracer accumulation from reconstructed PET images. First, the concentration of tracer emitters in a region of interest (ROI) of the target tissue is recovered at a given time, as the solution of an appropriately defined inverse problem. Next, the corresponding normalized radioactivity concentration is estimated by the SUV, which is defined as [1]

$$\text{SUV} = \frac{\text{activity concentration per unit mass [Bq/kg]}}{\text{injected activity [Bq]/ body mass [kg]}}.$$

According to this definition, the radioactivity concentration in the ROI is normalized to the radioactivity concentration in the body, which is estimated as the ratio between the injected activity and the patient body mass. There are slightly different definitions available; moreover, SUV measurements are affected by physiological and technological factors [1,3].

Overall, the SUV is an oversimplified index depending on the time interval between injection and observation, location and dimensions of the ROI, and uptake by other tissues [3]. Nevertheless, the localized SUV has been used to stage tumors and to assess response to therapies.

2.2. Input function

Tissues extract the tracer from blood. Indeed, only free FDG is available for tissue uptake, while the radioligand bound to blood cells and metabolites is firmly constrained to remain in blood [40,41]. In the present work, the concentration C_b of the tracer available for input to tissues is identified with the measured concentration in arterial blood, which means in particular that the bound tracer is disregarded. Considerations about bound tracer are discussed in [40].

Tracer is delivered to tissues via blood flow, so that the amount of tracer locally extracted by a tissue is highly dependent on the concentration of radioactivity in blood. Thus, the reconstruction of FDG kinetics requires the knowledge of the arterial plasma time-activity concentration curve of the tracer, which in turn provides an estimate of the radioactivity available for uptake. There are several ways for the determination of the time course of concentration: serial arterial sampling, which is independent of PET data acquisition; images of tracer concentration in blood pools [58], such as the left ventricle; a variety of statistical reconstruction methods [52].

In the present work the arterial plasma activity concentration curve is regarded as given and plays the role of input function (IF). We assume that the IF, as well as any other activity curve, has been corrected for tracer decay.

2.3. Activity concentration of target tissue

The tissue selected for measuring the activity concentration C_T [Bq/ml] is referred to as the target tissue (TT). The time course of C_T, also regarded as the tissue response, is obtained from the ROI analysis of a dynamic series of images (see, e.g., [6,55]). We recall that data are corrected for attenuation and, possibly, other systematic sources of error. Obviously, the reconstructed value of C_T is functionally dependent on the shape of IF, the

characteristics of the target tissue, the injected dose, and the physiologic conditions of the patient.

The activity concentration measured by a PET scanner results from superposition of various signals emitted, e.g., by tracer molecules carried by blood partially occupying the ROI volume, molecules dispersed in the interstitial tissue, free and phosphorylated molecules in cells. The analysis of these PET data aims at the reconstruction of the detailed kinetics of the tracer. In a sense, the measured signal has to be resolved into the activity pertaining to each source. To this aim, tracer kinetics takes into account the flow of radioactive molecules between the various sources. This is achieved by the application a mathematical models, as described in the next section. Comparison between model predictions and measured data leads to the determination of tracer kinetics, through solution of an inverse problem.

3. The construction of compartmental models

3.1. Generalities

Compartmental analysis provides a mathematical model relating PET data to specific metabolic states or chemical compounds of the tracer, while possibly taking into account their distribution in space. The metabolic states are known as compartments, sources, or pools. A fundamental requirement of compartmental modeling is the so-called well-mixed assumption, which means that the tracer distribution in each compartment is spatially homogeneous, and the tracer exchanged between compartments is instantaneously mixed. Further conditions for applicability of compartmental analysis are described in detail in the next subsection.

Each compartment is characterized by the related time dependent activity concentration. It is understood that different compartments, such as free and phosphorylated FDG, may occupy the same spatial volume; conversely, if a chemical compound of the tracer occupies volumes separated by a membrane, as occurs to free tracer in interstitial tissue and cytosol, then the compound may be associated with two spatially distinct compartments of possibly different concentrations.

A compartmental model (CM) is given by an interconnected set of compartments. The number of compartments to consider depends on the chemical, physiological, and biological properties of the tracer to model [6,25,54]. By adopting a compartmental approach, complex physiological systems are reduced to a finite number of basic constituents. Notice that, in principle, blood should be considered as a compartment, but in the present description it is not regarded as such because the corresponding concentration of tracer is viewed as known through measurements [55].

The concentrations of the various pools are the state variables of the CM, their time dependence being determined by tracer exchange. The tracer flux between compartments, e.g. from the free to the phosphorylated pool, occurs according to mass conservation. Usually, it is assumed that the outgoing flux depends on the concentration of the source.

The time rate of the concentration of each compartment is set equal to the difference between the tracer that enters and leaves the compartment per unit time and unit volume. Application of the conservation law shows that concentrations are related by a system of ordinary differential equations (ODEs). The IF is the forcing function of the system, providing tracer supply to the interconnected compartments. Here it is assumed that all the initial concentrations vanish, because there is no tracer available at the beginning of each experiment. According to this mathematical model, the state variables are the solutions of a Cauchy problem. In fact, we consider linear ODEs with constant rate coefficients, representing the rate of flux of tracer between compartments, say, the rate of phosphorylation of FDG molecules. The constants are also termed transfer coefficients or microparameters [17]. If the rate coefficients and the initial state are given, then the solution of the Cauchy problem provides a detailed description of tracer kinetics. However, typical problems of compartmental analysis require the determination of the rate constants such

that the corresponding solution complies with the overall measured tissue concentration. From the viewpoint of mathematics, this is a typical inverse problem. As a first step in the solution of the inverse problem, it must be shown that the rate coefficients are uniquely determined by the available data. This requirement puts severe limitations on the number of coefficients allowed, and hence on the number of compartments/metabolic states and the related interconnections to consider. The result is a sort of trade-off between the need for simplification in the formal description and exhaustiveness in the representation of reality. Here we consider models resulting from one to three compartments.

In the course of this section we first recall the basic conditions needed to ensure the applicability of compartmental analysis. The general reference framework has been described by the previous discussion, which also provides some motivation. Next, we examine a few CMs, which are of rather common use, and hence are regarded as highly significant. Particular attention is devoted to the formulation of the inverse problem equation (IPE), which provides the starting point for the formulation of the inverse problem, whose solution determines the kinetics of the tracer. Finally, we introduce a compact (matrix) form of CMs, we present the formal solution of the direct problem, and we write down the IPE in a general form.

3.2. Basic applicability conditions

In a typical PET experiment a fraction of tracer is adsorbed by tissues after injection into blood, while some tracer is lost by tissues and poured back into blood. The previous discussion has indicated that application of compartmental analysis allows a reliable reconstruction of tracer kinetics, but this can be achieved only if a certain number of conditions are satisfied in the course of the experiment [2,6,32,41,55]. The following list describes the most common and relevant requirements.

- Tracer is administered in trace amounts. The number of injected molecules is supposed to be sufficiently high so that diffusion may described by application of a continuous model. However, such a number is not so high as to influence physiological processes and molecular interactions. In particular, tracer does not affect glucose metabolism.
- During an experiment, physiologic conditions are in a steady state which is not affected by measurement devices of tracer concentration. This holds true, in particular, for glucose metabolism.
- The well-mixing condition holds for each compartment. In practice, this means that equilibrium is reached in a time interval, which is rather short with respect to the time of data acquisition. As a consequence, also the spatial homogeneity condition follows, which implies that the tracer concentration in each compartment depends only on time.
- Transport of tracer molecules and related composites between compartments follows a first order kinetics, which ultimately leads to linear ODEs.
- Bound tracer in blood is disregarded, and the arterial concentration of tracer available for tissue uptake is regarded as a valuable approximation of capillary concentration.

We have described general assumptions underlying most used compartmental models. More specific aspects of tracer kinetics may be considered in order to generate highly realistic models. For example, a distinction may be introduced between free interstitial tracer and free intracellular tracer; permeabilities of blood vessels and cellular membranes may be considered, as well as dependence of activity on spatial variables. CMs explicitly devoted to the modeling of particular physiologic conditions will be examined in a subsequent section.

3.3. Examples of standard CMs

The following examples are itemized according to growing complexity. We adopt typical notations and conventions of the nuclear medicine framework. To simplify, compartments and corresponding concentrations [MBq/ml] are denoted by capital letters $\mathcal{C}_a$ and C_a, respectively, where the low index a identifies the specific compartment. Rate

constants [min^{-1}] are denoted by k_b, where the low index refers to the specific function in the set of interconnected compartments. Equal low indexes in different compartment models correspond to the same interpretation; at each step, interpretations already discussed for the previous steps are not repeated. We recall that, unless otherwise specified, the initial state is always considered at vanishing concentrations. In figures, compartments are denoted as boxes; by a slight abuse, the same box notation is adopted for the blood compartment; arrows represent flux of tracer between compartments; superposed indexed letters identify the rate constants.

3.3.1. 1-compartment model

The 1-compartment model (1-CM) was proposed in order to quantify blood perfusion [2,55]; recently, it has also been applied to describe tracer exchange during the flow of blood through a capillary [31].

The 1-CM is an oversimplified model where there is only one tissue compartment $\mathcal{C}_f$ with state variable C_f, accounting for the overall tracer content. The concentration C_b of the IF is given. The differential equation for C_f is

$$\dot{C}_f = -k_2\, C_f + k_1\, C_b\,, \tag{1}$$

where k_1 and k_2 are the rate constants for the incoming and outgoing tracer. In other words, $k_1\, C_b$ is the rate of the incoming flow of tracer per unit volume, while $k_2\, C_f$ is the analogous rate of the outgoing flow; thus, the net rate of tracer concentration per unit volume, $\dot{C}_f$, is the difference $k_1 C_b - k_2 C_f$, consistently with conservation of the tracer mass. Notice explicitly that the plus and minus signs refer systematically to incoming and outgoing flows, respectively, for the compartment considered. The case $k_2 = 0$ corresponds to irreversible uptake, which means that tracer cannot escape from the compartment.

The solution of equation (1) (vanishing at $t = 0$) is

$$C_f = k_1 \int_0^t e^{-k_2\,(t-\tau)}\, C_b(\tau)\, d\tau. \tag{2}$$

Therefore, the concentration C_f is proportional to k_1, which is related to the absorption capacity of the tissue. The parameter $1/k_2$ is related to the asymptotic equilibrium time. For example, in the case $C_b(t) = \bar{C}$ constant, it is found that $C_f = h\,(1 - e^{-k_2\, t})$, where $h = \bar{C}\, k_1/k_2$ denotes the asymptotic equilibrium value. If $t = 1/k_2$, it is found that $C_f = 0.63\, h$, rather close to the asymptotic value.

Consider the measured activity concentration per unit volume, C_T. This PET measurement is set equal to the weighted sum of the free tracer activity concentration in tissue and a contribution arising from the distributed blood and vessels, of the same concentration C_b as that of the whole blood. Thus we have

$$C_T = (1 - V_b)\, C_f + V_b\, C_b\,, \tag{3}$$

where the dimensionless parameter V_b denotes the volume fraction of tissue occupied by blood. Replacing (2) into (3) provides the IPE for the 1-CM for the unknown rate constants k_1 and k_2.

3.3.2. 2-compartment model

Standard compartmental models have been developed under the assumption that the intracellular processes of phosphorylation and dephosphorylation of FDG are modeled by the use of two compartments $\mathcal{C}_f$ and $\mathcal{C}_p$, accounting for free and phosphorylated tracer, respectively (see, e.g., [48,55]). In 2-compartment models (2-CMs), the state variables are

the concentrations C_f and C_p. The linear system of ODEs involves four rate constants, and is written as

$$\dot{C}_f = -(k_2 + k_3)\, C_f + k_4\, C_p + k_1\, C_b, \tag{4}$$

$$\dot{C}_p = k_3\, C_f - k_4\, C_p. \tag{5}$$

The two equations express the conservation of tracer exchanged between the compartments $\mathcal{C}_f$ and $\mathcal{C}_p$. Thus, the outgoing flux $-k_3\, C_f$ from $\mathcal{C}_f$ in (4) corresponds to the incoming flux $k_3\, C_f$ into $\mathcal{C}_p$ in (5). Similar remarks hold for the flux $k_4\, C_p$. The constants k_3 and k_4 are related to phosphorylation and dephosphorylation rates, respectively, resulting from the action of the enzymes HK and G6Pase. Again, k_1 and k_2 are the rate constants for the incoming and outgoing tracer between the compartment $\mathcal{C}_f$ and blood.

The case $k_4 \neq 0$ is usually referred to as the reversible 2-CM, since tracer is allowed to leave the compartment $\mathcal{C}_p$. Conversely, the case $k_4 = 0$ corresponds to the irreversible 2-CM, in the sense that dephosphorylation does not occur and hence tracer is trapped inside $\mathcal{C}_p$; as a consequence, the corresponding concentration C_p grows in time. In general, a compartmental system is said to be irreversible if it contains at least one irreversible compartment; otherwise, it is called reversible. The irreversible 2-CM was considered first in a seminal paper by Sokoloff *et al* [48]. A great number of reconstruction of rate constants performed over years have shown that, in general, the value of k_4 is relatively small, so that the irreversible 2-CM is often regarded as a mathematical model providing a satisfactory approximation of tracer kinetics.

For later convenience, we observe that the solution of the system (4), (5) in the irreversible case ($k_4 = 0$) takes the form

$$C_f = k_1 \int_0^t e^{-(k_2+k_3)\,(t-\tau)}\, C_b(\tau)\, d\tau \tag{6}$$

$$C_p = \frac{k_1\, k_3}{k_2 + k_3} \int_0^t C_b\, d\tau - \frac{k_3}{k_2 + k_3}\, C_f\,. \tag{7}$$

The solution of the system (4), (5) in the reversible case ($k_4 \neq 0$) is given as

$$C_f = \frac{k_1}{\lambda_1 - \lambda_2} \Big[(k_4 + \lambda_1)\, \mathcal{I}_1 - (k_4 + \lambda_2)\, \mathcal{I}_2 \Big] \tag{8}$$

$$C_p = \frac{k_1\, k_3}{\lambda_1 - \lambda_2} \Big[\mathcal{I}_1 - \mathcal{I}_2 \Big]. \tag{9}$$

where

$$\mathcal{I}_1 = \int_0^t e^{\lambda_1\,(t-\tau)}\, C_b(\tau)\, d\tau, \qquad \mathcal{I}_2 = \int_0^t e^{\lambda_2\,(t-\tau)}\, C_b(\tau)\, d\tau \tag{10}$$

with

$$\lambda_{1,2} = [-(k_2 + k_3 + k_4) \pm \sqrt{\Delta}]/2, \tag{11}$$

and

$$\Delta = (k_2 + k_3 + k_4)^2 - 4\, k_2\, k_4 = (k_2 + k_3 - k_4)^2 + 4\, k_3\, k_4.$$

In other words, the concentrations are expressed as linear combination of the integrals $\mathcal{I}_1$ and $\mathcal{I}_2$, with coefficients depending on the rate constants.

The connection between the mathematical model and the PET data is given by the IPE

$$C_T = (1 - V_b)\, (C_f + C_p) + V_b\, C_b. \tag{12}$$

The concentration C_T in the left side of (12) refers to the total activity of the target tissue, reconstructed from the analysis of PET images; the contribution $V_b\, C_b$ in the right side comes from tracer molecules in blood, while $(1 - V_b)\, (C_f + C_p)$ comes from tracer molecules in tissue cells: here C_b is given, while C_f and C_p are the formal solutions of the system

of ODE, expressed in either the irreversible form (6), (7), or the reversible form (8), (9) . Overall, equation (12) expresses the fact that the measured tracer concentration, in the ROI considered, results from FDG molecules in blood, and free and phosphorylated FDG in tissue and molecules.

We point out that there are situations where the tracer content of blood may be disregarded, which corresponds to setting $V_b = 0$. Conversely, if needed, the volume fraction V_b may be regarded as an additional unknown parameter.

3.3.3. 3-compartment model

Biochemistry arguments show that G6Pase is anchored to the endoplasmic reticulum (ER) [14], so that its action of hydrolysis of G6P and FDG6P, resulting in the creation of a phosphate group and free molecules of glucose and FDG, occurs after transport of the phosphorylated forms into ER by the transmembrane protein glucose-6-phosphate transporter (G6PT) [30]. Subsequently, free FDG in ER may be released in cytosol. Further biochemical, pharmacological, clinical, and genetic data lead to a natural interpretation of ER as a distinct metabolic compartment [10].

Driven by biochemical reactions involving FDG molecules, a 3-compartment model (2-CM) has been developed, which is formed by the following compartments: $\mathcal{C}_f$, accounting for free tracer in the cytosol and possibly in the interstitial space, $\mathcal{C}_p$ for phosphorylated FDG in cytosol, and $\mathcal{C}_r$ for phosphorylated FDG in ER [44,49]. The standard compartmental 2-CM is recovered from the 3-CM under the assumption that the ER compartment is removed.

3-CM has been applied to the reduction of data coming from *in vitro* [44] and *in vivo* [49] experiments. Although we deal with the same set of three compartments, the resulting models and the related approaches differ in various significant aspects. For example, the process of data acquisition *in vitro* requires the use of a dedicated device (Ligand Tracer) with a properly defined calibration process, while activities replace concentrations as state variables [44,49]. However, the most outstanding result obtained from the mathematical analysis of data via 3-CM, i.e. that tracer is accumulated in ER, holds both *in vitro* and *in vivo* and this has been confirmed by the localization of fluorescent FDG analogues in the case of *in vitro* experiments [44].

Coherently with the general approach of this review, in this section we restrict our attention to applications of 3-CM to the analysis of *in vivo* data.

The state variables are the concentrations C_f, C_p, and C_r. The system of ODEs is given by

$$\dot{C}_f = -(k_2 + k_3)\, C_f + k_6\, C_r + k_1\, C_b, \tag{13}$$

$$\dot{C}_p = k_3\, C_f - k_5\, C_p, \tag{14}$$

$$\dot{C}_r = k_5\, C_p - k_6\, C_r. \tag{15}$$

The rate constant k_5 is related to tracer transport across the membrane of the ER, or the action of the transporter G6PT. The parameter k_6 is related to dephosphrylation by G6Pase; thus it may be regarded as the correspondent of k_4 in the 2-CM system. Since dephosphorylation occurs only inside ER, the parameter k_4, which corresponds to a flux from $\mathcal{C}_p$ to $\mathcal{C}_f$, is set equal to 0.

Following the previous definitions, the case $k_6 \neq 0$ is referred to as the reversible 3-CM, since tracer is allowed to leave the ER after dephosphorylation. Conversely, the case $k_6 = 0$ corresponds to the irreversible 3-CM: dephosphorylation does not occur and the tracer cannot leave the ER compartment.

For later reference, we observe that the solution of the irreversible version ($k_6 = 0$) of the system (13)–(15) may be written as

$$C_f = k_1 \int_0^t e^{-(k_2+k_3)\,(t-\tau)}\, C_b(\tau)\, d\tau, \tag{16}$$

$$C_p = k_3 \int_0^t e^{-k_5\,(t-\tau)}\, C_f(\tau)\, d\tau, \tag{17}$$

and

$$C_r = k_5 \int_0^t C_p(\tau)\, d\tau\,. \tag{18}$$

The connection between the tracer concentration C_T estimated over a suitable ROI and the formal solution of the ODEs (13)-(15) is obtained as follows [49]. The volume $\mathcal{V}_{\text{tot}}$ of the ROI is partitioned as

$$\mathcal{V}_{\text{tot}} = \mathcal{V}_{\text{int}} + \mathcal{V}_{\text{cyt}} + \mathcal{V}_{\text{er}} + \mathcal{V}_{\text{blood}}\,, \tag{19}$$

where $\mathcal{V}_{\text{blood}}$ and $\mathcal{V}_{\text{int}}$ denote the volume occupied by blood and interstitial fluid, respectively; $\mathcal{V}_{\text{cyt}}$ and $\mathcal{V}_{\text{er}}$ denote the total volumes of cytosol and ER in tissue cells. The total activity $\mathcal{V}_{\text{tot}}\mathcal{C}_T$ in $\mathcal{V}_{\text{tot}}$ is related to the state variables and the IF by

$$\mathcal{V}_{\text{tot}}C_T = \mathcal{V}_{\text{int}}C_f + \mathcal{V}_{\text{cyt}}C_f + \mathcal{V}_{\text{cyt}}C_p + \mathcal{V}_{\text{er}}C_r + \mathcal{V}_{\text{blood}}C_b\,. \tag{20}$$

The volume fractions of blood and interstitial fluid are defined as

$$V_b = \frac{\mathcal{V}_{\text{blood}}}{\mathcal{V}_{\text{tot}}}\,, \qquad V_i = \frac{\mathcal{V}_{\text{int}}}{\mathcal{V}_{\text{tot}}}\,, \tag{21}$$

and the further dimensionless parameter v_r as

$$v_r = \frac{\mathcal{V}_{\text{er}}}{\mathcal{V}_{\text{cyt}} + \mathcal{V}_{\text{er}}}. \tag{22}$$

Notice that v_r is independent of the number of cells and may be estimated as the ratio of the ER volume and the sum of the cytosolic and reticular volumes of any cell. It is found that

$$\frac{\mathcal{V}_{\text{er}}}{\mathcal{V}_{\text{tot}}} = v_r(1 - V_b - V_i)\,, \qquad \frac{\mathcal{V}_{\text{cyt}}}{\mathcal{V}_{\text{tot}}} = (1 - v_r)(1 - V_b - V_i)\,. \tag{23}$$

Accordingly, equation (20) may be written in the equivalent form

$$C_T = \alpha_1\, C_f + \alpha_2\, C_p + \alpha_3\, C_r + V_b\, C_b\,, \tag{24}$$

which is the IPE of 3-CM and where the positive dimensionless constants α_1, α_2, and α_3 are defined as

$$\alpha_1 = V_i + (1 - v_r)(1 - V_b - V_i)\,, \tag{25}$$

$$\alpha_2 = (1 - v_r)(1 - V_b - V_i)\,, \tag{26}$$

$$\alpha_3 = v_r(1 - V_b - V_i)\,. \tag{27}$$

Remark: As intentionally suggested by similarities in notation, 2-CM is a simplification of 3-CM. It has already been observed that the rate constant k_6 in 3-CM corresponds to k_4 in 2-CM, in that both parameters are related to the process of dephosphorylation of the tracer molecules.

More in general, there are various possibilities of analyzing the correspondence between models from a formal viewpoint. For example, consider the system of ODE for 3-CM and suppose that C_p is almost constant. Indeed, repeated applications of 3-CM have shown that C_p reaches a stationary value after a very short transition time [44,49]. In that case, equation (14) reduces to $k_3\, C_f = k_5\, C_p$ (as a consequence, also C_f becomes constant, consistently with simulations). After substitution of this condition, (14) takes the form

$$\dot{C}_r = k_3\, C_f - k_6\, C_r. \tag{28}$$

Equations (13) and (28) coincide with (4) and (5) of 2-CM, provided C_r and k_6 are identified with C_p and k_4, respectively. This is also consistent with the observation that accumulation of FDG occurs in ER, rather than cytosol [44,49]. In a sense, a stable amount of phosphorylated tracer remains in cytosol, providing a similarly stable flux $k_5\, C_p = k_3\, C_f$ towards ER. A further point to consider while connecting the two models is related to the fact that phosphorylated tracer in 2-CM occupies the volume $\mathcal{V}_{\rm cyt}$ while C_r in 3-CM occupies the volume $\mathcal{V}_{\rm er}$.

3.4. Compact formulation and general formal solution of the direct problem

We describe an alternative formulation of the ODEs for CMs which is given in matrix form, and is used in a number of developments. This compact formulation writes

$$\dot{\boldsymbol{C}} = \boldsymbol{M}\,\boldsymbol{C} + k_1\, C_b\, \boldsymbol{e} \tag{29}$$

In general, $\boldsymbol{C}$ is the n-dimensional column vector of state variables; $\boldsymbol{M}$ is a constant square matrix of order n, with entries given by the rate coefficients; $\boldsymbol{e}$ is a constant n-dimensional column vector. Addition of the initial condition $\boldsymbol{C}(0) = 0$ gives rise to a Cauchy problem for the unknown state vector $\boldsymbol{C}$. We refer to its solution as the solution of the direct problem.

For 2-CM, comparison with (4), (5) shows that

$$\boldsymbol{M} = \begin{bmatrix} -(k_2 + k_3) & k_4 \\ k_3 & -k_4 \end{bmatrix}, \quad \boldsymbol{C} = \begin{bmatrix} C_f \\ C_p \end{bmatrix}, \quad \boldsymbol{e} = \begin{bmatrix} 1 \\ 0 \end{bmatrix}. \tag{30}$$

Notice that the matrix $\boldsymbol{M}$ is singular for irreversible models; conversely, $\boldsymbol{M}$ is non-singular with eigenvalues λ_1 and λ_2 from equation (11) for reversible models. Similarly, the system (13)–(15) for 3-CM is written in the form (29) with

$$\boldsymbol{M} = \begin{bmatrix} -(k_2 + k_3) & 0 & k_6 \\ k_3 & -k_5 & 0 \\ 0 & k_5 & -k_6 \end{bmatrix}, \quad \boldsymbol{C} = \begin{bmatrix} C_f \\ C_p \\ C_r \end{bmatrix}, \quad \boldsymbol{e} = \begin{bmatrix} 1 \\ 0 \\ 0 \end{bmatrix}. \tag{31}$$

The general structure and properties of the system matrix $\boldsymbol{M}$ have been extensively discussed, e.g. in [19,42]. We only observe that if the system is irreversible then there is at least one compartment, say $\mathcal{C}_n$, such that the tracer cannot get out. This is equivalent to the statement that the diagonal element M_{nn} of the matrix $\boldsymbol{M}$ vanishes. As an immediate consequence of (30) and (31), the system matrix of irreversible 2-CMs and 3-CMs is singular. The result holds in general for irreversible CMs.

The solution of the direct problem may be represented as

$$\boldsymbol{C}(t; \boldsymbol{k}, C_b) = k_1 \int_0^t e^{\boldsymbol{M}\,(t-\tau)}\; C_b(\tau)\, d\tau\, \boldsymbol{e}, \tag{32}$$

where $\boldsymbol{k}$ is the vector of parameters defined as $\boldsymbol{k} = (k_1, k_2, \ldots, k_m)^T$, with upper T denoting the transpose and $\boldsymbol{M}$ depending on the CM adopted. The notation gives evidence to the dependence of $\boldsymbol{C}$ on the rate constants and the input function.

The compact form of the IPE is given by

$$C_T = \boldsymbol{\alpha}\, \boldsymbol{C}(t; \boldsymbol{k}, C_b) + V_b\, C_b, \tag{33}$$

where $\boldsymbol{\alpha}$ is a constant row vector of order n, with components possibly depending on the physiological parameters. Equation (33) reduces to (12) for 2-CM if $\boldsymbol{\alpha} = [1 - V_b, 1 - V_b]$. Similarly, we recover equation (24) for 3-CM by letting $\boldsymbol{\alpha} = [\alpha_1, \alpha_2, \alpha_3]$.

Replacing expression (32) of $\boldsymbol{C}$ into (33) provides the IPE governing the inverse problem for the unknown vector $\boldsymbol{k}$, at given C_T and C_b.

Remark: In the present approach we have described a rather simple and essential formulation of compartmental analysis, which however is sufficient to deal with standard

applications in nuclear medicine. In more general situations, tracer could be delivered from blood to more than one compartment, with different time rate constants, which implies a change in the definition of the vector $\boldsymbol{e}$. Furthermore, we have assumed that the observed activity results from the superposition of the activities of all tissue compartments, but it may happen that more than one, say h outputs, could be observed, so that the IPE should be replaced by a system of h equations.

4. Patlak and Logan graphical approaches

Graphical methods are essentially based on the following observation. Two appropriate functions of the measurements identify the parametric representation of a time dependent plane curve which becomes linear for large time values. Application of a linear regression method to the plot provides an estimate of a corresponding slope, which can be given an interpretation in terms of either tracer absorption (irreversible CMs) or tracer distribution (reversible CMs). In other words, graphical methods may be regarded as procedures for the solution of a simplified inverse problem, yielding useful information on the overall tracer kinetics.

Here we describe the Patlak graphical approach (PGA) and the Logan graphical approach (LGA) which apply to irreversible and reversible CMs, respectively [27,36]. The procedure leading to the generation of the asymptotically linear curves follows from the properties of the specific CM, but the final parametric equation of the curve depends only on the available data. Therefore, we first describe the algorithm for the construction of the (asymptotically linear) curves for irreversible CMs, and we show how it works by application to a 2-CM and a 3-CM. A general approach to reversible CMs is then proposed, with specific examples.

4.1. PGA

PGA provides a useful consequence of the IPE holding for a family of irreversible CMs, in that it is used to estimate the net influx rate of radiotracer at large time values. Subsequent multiplication by the so-called lumped constant provides an estimate of the rate of glucose uptake [44]. The general process for deriving PGA is described in the following procedure, which is divided into three steps, for the sake of clarity. Then, applications to 2-CM and 3-CM will be described.

- **First step.** The vector solution $\boldsymbol{C}$ of the irreversible system of ODE (29) is substituted into the IPE (33), which is then divided by C_b. The resulting equation takes the form

$$\frac{C_T}{C_b} = \alpha_P \frac{\int_0^t C_b}{C_b} + \beta_P(t), \tag{34}$$

  (see the Appendix) where α_P [min^{-1}] is a constant macroparameter [17], and β_P depends on C_b and the components of $\boldsymbol{C}$.
- **Second step.** In a number of relevant cases it may be shown that β_P is asymptotically constant. Then, in the plane referred to Cartesian coordinates (x, y), define the functions $x(t)$ and $y(t)$ by

$$x(t) = \frac{\int_0^t C_b}{C_b}, \qquad y(t) = \frac{C_T}{C_b}, \tag{35}$$

  $t \in (0, \infty)$. The points $(x(t), y(t))$ give the parametric representation of a curve which is known as the standard Patlak plot [62]. Comparison with equation (34) and the condition on β_P show that the curve is asymptotically linear. Thus the slope α_P and the adimensional constant intercept β_P are estimated in terms of the data by linear regression [62]. The procedure may be applied pixel-wise.
- **Third step.** The interpretation of α_P is achieved by comparison with the stationary solution of the system of ODEs (29), corresponding to a constant IF. It is shown that

α_P measures the rate of tracer uptake by the tissue at stationary conditions.

The general proof of the procedure is given in the Appendix. Here we show how and why it works by considering in detail irreversible 2-CMs and 3-CMs.

4.1.1. PGA for 2-CM

Consider an irreversible 2-CM system: the concentrations C_f and C_p are given by (6) and (7), so that $C_f + C_p$ takes the form

$$C_f + C_p = \frac{k_1\, k_3}{k_2 + k_3} \int_0^t C_b\, d\tau + \frac{k_2}{k_2 + k_3}\, C_f\,. \tag{36}$$

Replacing this expression into the IPE (12)and then dividing by C_b, leads to (34) with

$$\alpha_{P2} = (1 - V_b)\frac{k_1\, k_3}{k_2 + k_3}, \tag{37}$$

and

$$\beta_{P2}(t) = (1 - V_b)\, \frac{k_2}{k_2 + k_3}\, \frac{C_f}{C_b} + V_b, \tag{38}$$

where the suffix $P2$ refers to the PGA for the 2-CM.

Following Step 2, we observe that if the ratio C_f/C_b is asymptotically constant, then the adimensional quantity β_{P2} is constant as well, for large t values, and the Patlak plot is asymptotically linear. It may be shown that constancy of C_f/C_b occurs in two remarkable cases: when the IF C_b is (asymptotically) constant or exponentially decaying. The latter condition may be regarded as typical for tracer concentration in plasma [52].

According to Step 3, the direct interpretation of α_{P2} is obtained as follows. Consider the system (4), (5) in the irreversible case ($k_4 = 0$), suppose that the IF C_b is constant, and look for stationary solutions. Denote by an upper star the constant values. From the system of ODES it follows that C_f and $\dot{C}_p$ assume constant values. Specifically, we find

$$C_f^* = \frac{k_1}{k_2 + k_3}\, C_b^*, \qquad \dot{C}_p^* = \frac{k_1\, k_3}{k_2 + k_3}\, C_b^*. \tag{39}$$

Replacing expression (39) of $\dot{C}_p^*$ in the time derivative of the IPE (12), and comparing the result with the definition of α_{P2} shows that

$$\dot{C}_T^* = \alpha_{P2}\, C_i^*. \tag{40}$$

We conclude that C_T grows at the constant rate $\alpha_{P2}\, C_i^*$. In words, $\alpha_{P2}\, C_i^*$ represents the net tracer rate uptaken by the tissue in stationary conditions; it may be estimated directly from data, without explicit knowledge of the values of the rate constants. A pixel by pixel evaluation is also allowed. Finally, we remark that the rate of FDG uptake has been used to estimate glucose uptake through multiplication by the lumped constant [6,44,48].

Remark: The coefficient α_P is obtained by re-writing the IPE (33) in the form of the Patlak plot. Since in general (33) depends on the volume fraction, the same holds for α_{P2}, as brought into evidence by definition (37). The slope coefficient α_{P2}, which is related to the rate of tracer uptake, comes from application of linear regression to the whole Patlak curve, with t varying from 0 to ∞. The coefficient α_{2P} is different from the slope of the line asymptotically approximating the Patlak curve [62]. This remark holds independently of the number of compartments.

Remark: A required condition for application of PGA is that $k_4 = 0$. Nevertheless, it is rather common to use PGA for 2-CMs in order to estimate the rate of tracer uptake. To discuss here the feasibility of this approach, we look at IPE for small values of k_4. We show that the sum $C_f + C_p$ converges to the expression of the irreversible case ($k_4 = 0$) for $k_4 \to 0$. In words, the reversible model converges to the irreversible one, as to the

formulation of IPE. Thus, the value of the accumulation rate obtained by application of the irreversible model (which coincides with α_{P2}) may be interpreted as an approximation of the overall tracer uptake rate for small k_4.

Suppose now that $k_4 \neq 0$. According to (8) and (9) we have

$$C_f + C_p = \frac{k_1}{\lambda_1 - \lambda_2}\left[(k_3 + k_4 + \lambda_1)\,\mathcal{I}_1 - (k_3 + k_4 + \lambda_2)\,\mathcal{I}_2\right]$$

. Further, accounting for the definitions, we find that

$$\lambda_1 \to 0, \qquad \lambda_2 \to -(k_2 + k_3), \qquad \lambda_1 - \lambda_2 \to (k_2 + k_3)$$

,

$$\mathcal{I}_1 \to \int_0^t C_b, \qquad k_1\,\mathcal{I}_2 \to k_1 \int_0^t e^{-(k_2+k_3)\,(t-\tau)} C_b(\tau)\,d\tau = C_{f,k_4=0}$$

for $k_4 \to 0$; in particular $C_{f,k_4=0}$ refers to the expression (6) of C_f, evaluated at $k_4 = 0$. It follows that

$$C_f + C_p \to \frac{k_1\,k_3}{k_2 + k_3}\int_0^t C_b\,d\tau + \frac{k_2}{k_2 + k_3}\,C_{f,k_4=0} \qquad (k_4 \to 0),$$

which corresponds to equation (36) and which leads to the Patlak plot. Thus the estimate of the rate of tracer uptake α_{P2} by application of the PGA is taken as an approximate estimate of the rate in the presence of a small dephosphorylation effect.

4.1.2. PGA for 3-CM

Consider now the irreversible 3-CM. To accomplish Step 1, equation (24) is re-written in the equivalent form

$$C_T = (\alpha_1 - \alpha_3)\,C_f + (\alpha_2 - \alpha_3)\,C_p + \alpha_3(C_f + C_p + C_r) + V_b C_b. \tag{41}$$

Next, the sum of the differential equations (13), (14), and (15) is re-written as

$$\frac{d}{dt}(C_f + C_p + C_r) = -k_2\,C_f + k_1\,C_b$$

. Evaluation of the integral from 0 to t, and substitution of the explicit expression of C_f from (16) leads to

$$C_f + C_p + C_r = \frac{k_1\,k_3}{k_2 + k_3}\int_0^t C_b + \frac{k_2}{k_2 + k_3}\,C_f\,. \tag{42}$$

Replacing the expression (42) into (41), and dividing by C_b leads to the standard equation for the Patlak plot (34), where

$$\alpha_{P3} = \alpha_3\,\frac{k_1\,k_3}{k_2 + k_3}\,, \tag{43}$$

$$\beta_{P3}(t) = (\alpha_1 - \alpha_3 + \frac{k_2}{k_2 + k_3})\,\frac{C_f}{C_b} + (\alpha_2 - \alpha_3)\,\frac{C_p}{C_b} + V_b\,. \tag{44}$$

According to Step 2, if β_{P3} is asymptotically constant then an asymptotically linear Patlak plot is obtained.

Step 3 provides the interpretation of α_{P3}. In fact, consider the system of ODEs (13)–(15), under the assumption of irreversibility ($k_6 = 0$) and look for stationary solutions at constant $C_b = C_b^*$. It is found, in particular, that

$$\dot{C}_r^* = \frac{k_1\,k_3}{k_2 + k_3}\,C_b^*.$$

Evaluation of the asymptotic value of the time derivative of the IPE (24) shows that

$\dot{C}_T^* = \alpha_3 \dot{C}_r^*$. Substitution of the previous expression of $\dot{C}_r^*$ and comparison with the definition of α_{P3} leads to

$$\dot{C}_T^* = \alpha_{P3} C_b^*. \tag{45}$$

In words, C_T grows at the constant rate $\alpha_{P3} C_b^*$.

Remark: Equation (45) for 3-CM is the analog of (40) for 2-CM. This is consistent with the general discussion of PGA for irreversible CMs of generic order n, which is given in the Appendix.

As exemplified by equations (37) and (43), the explicit form of the equation connecting the general slope α_P to the microparameters depends on the structure of the CM. Indeed, PGA is model-independent, but requires the use of CMs for its motivation, development, proof.

4.2. LGA

Under suitable assumptions, LGA provides a useful consequence of IPE, which holds for reversible CMs; specifically, we obtain the estimate of a macroparameter representing a ratio between equilibrium concentrations. The procedure is somehow similar to that of §4.1 for PGA; we reproduce here the main steps in the case of a general reversible CM [27,40,54].

- **Step 1.** Consider the integral in time of the IPE equation in the compact form (33):

$$\int_0^t C_T = \int_0^t \boldsymbol{\alpha}\, \boldsymbol{C} + V_b \int_0^t C_b. \tag{46}$$

where $\boldsymbol{\alpha}\, \boldsymbol{C}$ is related to data through the ODE (29). Indeed, multiplication of (29) by $\boldsymbol{M}^{-1}$ yields

$$\boldsymbol{C} = \boldsymbol{M}^{-1} \dot{\boldsymbol{C}} - k_1 \boldsymbol{M}^{-1} \boldsymbol{e}\, C_b.$$

Further multiplication by $\boldsymbol{\alpha}$, and integration with respect to time from 0 to t gives

$$\int_0^t \boldsymbol{\alpha}\, \boldsymbol{C}(\tau;\boldsymbol{k})\, d\tau = \boldsymbol{\alpha}\, \boldsymbol{M}^{-1} \boldsymbol{C} - k_1\, \boldsymbol{\alpha}\, \boldsymbol{M}^{-1}\, \boldsymbol{e} \int_0^t C_b\, d\tau$$

Substitution into (46), followed by division by C_T gives the necessary condition

$$\frac{\int_0^t C_T}{C_T} = \alpha_L \frac{\int_0^t C_b}{C_T} + \beta_L(t) \tag{47}$$

where the dimensionless constant α_L and the function $\beta_L(t)$ [min^{-1}] are defined as

$$\alpha_L = -k_1\, \boldsymbol{\alpha}\, \boldsymbol{M}^{-1}\, \boldsymbol{e} + V_b, \tag{48}$$

$$\beta_L(t) = \frac{\boldsymbol{\alpha}\, \boldsymbol{M}^{-1} \boldsymbol{C}}{C_T}. \tag{49}$$

- Following the analogy with the GPA approach of §4.1, in a number of relevant cases it may be shown that β_L is asymptotically constant. In such a case, consider the functions $x(t)$ and $y(t)$ defined by

$$x(t) = \frac{\int_0^t C_b}{C_T}, \qquad y(t) = \frac{\int_0^T C_T}{C_T}, \tag{50}$$

$t \in (0, \infty)$. In analogy with (34) the points $(x(t), y(t))$ of the Cartesian plane define a parametric representation of the standard Logan plot, which is an asymptotically linear curve. The adimensional slope α_L and the intercept β_L are macroparameters determined by the data, which are estimated by linear regression.
- The interpretation of α_L follows from the equilibrium solution of the system (29) at

constant IF C_b^*. The equilibrium state $\boldsymbol{C}^*$ is given by

$$\boldsymbol{C}^* = -k_1\,\boldsymbol{M}^{-1}\,\boldsymbol{e}\,C_b^*.$$

According to the IPE (33), the previous equation, and the definition of α_L it follows that

$$C_T^* = \boldsymbol{\alpha}\,\boldsymbol{C}^* + V_b\,C_b^* = -k_1\,\boldsymbol{\alpha}\,\boldsymbol{M}^{-1}\,\boldsymbol{e}\,C_b^* + V_b\,C_b^* = \alpha_L\,C_b^* \tag{51}$$

Thus, the slope $\alpha_L = C_T^*/C_b^*$ is the ratio between the constant equilibrium value of the total tissue concentration and the blood concentration.

Remark: It should be noticed that C_T^* takes into account the total tracer content of a tissue volume, which means that also the contribution due to the presence of blood is considered.

An alternative interpretation of α_L in terms of volumes is obtained as follows. Suppose $\mathcal{V}_T$ and $\mathcal{V}_b$ are tissue and blood volumes containing the same amount of radioactivity at the equilibrium concentrations. This means that

$$C_T^*\,\mathcal{V}_T = C_b^*\,\mathcal{V}_b\,, \tag{52}$$

whence it follows that

$$\frac{\mathcal{V}_b}{\mathcal{V}_T} = \frac{C_T^*}{C_b^*} = \alpha_L\,. \tag{53}$$

Accordingly, α_L may also be interpreted as the ratio between blood and tissue volumes containing the same amount of tracer at equilibrium concentrations. We conclude that α_L assesses the overall capability of the tissue to concentrate or dilute tracer in equilibrium conditions.

4.2.1. LGA for 2-CM

We consider a reversible 2-CM system ($k_4 \neq 0$). Explicit computations show that

$$k_1\,\boldsymbol{\alpha}\,\boldsymbol{M}^{-1}\,\boldsymbol{e} = -(1-V_b)\,\frac{k_1}{k_2}\,\Big(1+\frac{k_3}{k_4}\Big)$$

and

$$\boldsymbol{\alpha}\,\boldsymbol{M}^{-1}\,\boldsymbol{C} = -(1-V_b)\,\Big(\frac{k_3+k_4}{k_2\,k_4}\,C_f + \frac{k_2+k_3+k_4}{k_2\,k_4}\,C_m\Big).$$

Substitution into the definitions (54) and (55) leads to

$$\alpha_{L2} = (1-V_b)\,\frac{k_1}{k_2}\,\Big(1+\frac{k_3}{k_4}\Big) + V_b, \tag{54}$$

and

$$\beta_{L2}(t) = -(1-V_b)\,\Big[\frac{k_3+k_4}{k_2\,k_4}\,\frac{C_f}{C_T} + \frac{k_2+k_3+k_4}{k_2\,k_4}\,\frac{C_p}{C_T}\Big], \tag{55}$$

where the low index $L2$ refer to the Logan plot for 2-CMs.

Suppose that V_b is small enough to be negleted. Then α_{L2} reduces to $(k_1/k_2)\,(1 + k_3/k_4) = DV_T$, which is called the total distribution volume [2,23,40].

4.2.2. LGA for 3-CM

Consider a reversible 3-CM ($k_6 \neq 0$). Following the same procedure as §4.2.1, with $\boldsymbol{M}$, $\boldsymbol{\alpha}$, and $\boldsymbol{e}$ properly updated, it is found that

$$\frac{\int_0^t C_T}{C_T} = \alpha_{L3}\,\frac{\int_0^t C_b}{C_T} + \beta_{L3}(t) \tag{56}$$

with

$$\alpha_{L3} = \boldsymbol{\alpha}\, \boldsymbol{M}^{-1}\, \boldsymbol{e} + V_b = \frac{k_1}{k_2}\left(\alpha_1 + \alpha_2 \frac{k_3}{k_5} + \alpha_3 \frac{k_3}{k_6}\right) + V_b \tag{57}$$

$$\beta_{L3}(t) = \frac{\boldsymbol{\alpha}\, \boldsymbol{M}^{-1}\, \boldsymbol{C}}{C_T} = -\left(\frac{\alpha_1}{k_2} + \frac{\alpha_2\, k_3}{k_2\, k_5} + \frac{\alpha_3\, k_3}{k_2\, k_6}\right) \frac{C_f + C_p + C_r}{C_T} - \frac{\alpha_2}{k_5}\frac{C_p}{C_T} - \frac{\alpha_3}{k_6}\frac{C_p + C_r}{C_T} \tag{58}$$

If $\beta_{L3}(t)$ is asymptotically constant, then equation (56) provides a standard Logan plot with slope α_{L3}.

An analysis of the system (13)–(15) and equation (24) at constant values of C_f, C_p, C_r, and C_b shows that $\alpha_{L,3C}$ coincides with $C_T^*/C_b^* = \mathcal{V}_b/\mathcal{V}_T$ such that $C_T^*\, \mathcal{V}_T = C_b^*\, \mathcal{V}_b$.

5. Issues on the solvability of the inverse problem

The fundamental application of compartmental analysis deals with the reconstruction of tracer kinetics via estimate of the rate constants, which cannot be measured directly. A natural requirement is that the parameters that identify the mathematical model are uniquely defined, up to noise in the data. This is known as the identifiability problem. There are, at least, two reasons to asses identifiability [7]. Since the rate constants have a kinetic meaning, we are interested in knowing whether their values can be determined uniquely from the available experimental data. Moreover, we expect difficulties in the estimate of parameters of a non-identifiable model. The discussion of a few aspects of these problems is the main aim of the present section with a particular focus on linear compartment models. The analysis of identifiability for nonlinear compartmental systems, such as those arising when fluxes between compartments are modeled by the Michaelis-Menten law, is still an open problem. A comparison of currently available techniques for nonlinear model is beyond the scope of this review and can be found in [7].

5.1. Identifiability of linear CMs

In some scenarios many distinct models may exist equally fitting the recorded data [49]. Here we assume tha a linear compartmental model has been fixed by exploiting, e.g., some a priori information on the biochemical process under consideration. Additionally, we assume all the physiological parameters, such as the blood volume fraction V_b, to be known and we investigate the identifiability of the kinetic parameters $\boldsymbol{k}$.

A standard approach to discuss the identifiability of linear CMs consists in computing the Laplace transform of both sides of the IPE (33) and of the system of ODEs (29), leading to, respectively,

$$\tilde{C}_T(s) = \boldsymbol{\alpha}\, \tilde{\boldsymbol{C}}(s) + V_b\, \tilde{C}_b(s)\,, \tag{59}$$

and

$$(s\, \boldsymbol{I} - \boldsymbol{M})\, \tilde{\boldsymbol{C}}(s) = k_1\, \tilde{C}_b(s)\, \boldsymbol{e}\,, \tag{60}$$

where we have indicated by $\tilde{f}(s)$ the Laplace transform of a function $f(t)$ and we have assumed suitable regularity conditions.

Provided the matrix $(s\, \boldsymbol{I} - \boldsymbol{M})^{-1}$ is invertible, by computing the solution $\tilde{\boldsymbol{C}}(s)$ of the linear system (60) and substituting it into equation (59) we obtain

$$\frac{\tilde{C}_T(s) - V_b\, \tilde{C}_b(s)}{\tilde{C}_b(s)} = k_1 \boldsymbol{\alpha}(s\, \boldsymbol{I} - \boldsymbol{M})^{-1} \boldsymbol{e} = k_1 \frac{Q(s, \hat{\boldsymbol{k}})}{D(s; \hat{\boldsymbol{k}})}\,, \tag{61}$$

where $\hat{\boldsymbol{k}} = [k_2, ..., k_m]^T$, $D(s; \hat{\boldsymbol{k}}) := \det(s\, \boldsymbol{I} - \boldsymbol{M})$ is a polynomial of degree n in the variable s with coefficients depending on $\hat{\boldsymbol{k}}$, and similarly $Q(s; \hat{\boldsymbol{k}}) := \boldsymbol{\alpha}\, \mathrm{adj}(s\, \boldsymbol{I} - \boldsymbol{M})\, \boldsymbol{e}$ is a polynomial of degree up to $n-1$, $\mathrm{adj}(s\, \boldsymbol{I} - \boldsymbol{M})$ being the adjugate of the $n \times n$ matrix $(s\, \boldsymbol{I} - \boldsymbol{M})$. In the following we assume that $Q(s; \hat{\boldsymbol{k}})$ and $D(s; \hat{\boldsymbol{k}})$ are coprime and that they have leading coefficient equal to 1.

Any alternative set $\boldsymbol{h} = [h_1, ..., h_m]^T$ of kinetic parameters that satisfy the IPE (33) and the system of ODEs (29) for the recorded input function $C_b(t)$ and total concentration $C_T(t)$ must satisfy equation (61), with $\boldsymbol{k}$ replaced by $\boldsymbol{h}$. Since the left-side of equation (61) does

not depends on the value of the kinetic parameters, the following necessary condition holds

$$k_1 \frac{Q(s,\hat{\boldsymbol{k}})}{D(s;\hat{\boldsymbol{k}})} = h_1 \frac{Q(s,\hat{\boldsymbol{h}})}{D(s;\hat{\boldsymbol{h}})}. \tag{62}$$

By exploiting the fact that $Q(s,\hat{\boldsymbol{k}})$ and $D(s;\hat{\boldsymbol{k}})$ have leading coefficients equal to 1, it can be easily shown that equation (62) implies $k_1 = h_1$. Then, since $Q(s,\hat{\boldsymbol{k}})$ and $D(s;\hat{\boldsymbol{k}})$ are coprime, from equation (62) it follows that

$$Q(s,\hat{\boldsymbol{h}}) = Q(s;\hat{\boldsymbol{k}}), \qquad D(s,\hat{\boldsymbol{h}}) = D(s;\hat{\boldsymbol{k}}). \tag{63}$$

If these two equations imply $\hat{\boldsymbol{h}} = \hat{\boldsymbol{k}}$, then identifiability is proved. The actual implementation of this last step depends on the particular CM under consideration and may be rather involved when many compartments are included in the model.

As an illustrative example, we consider a reversible 2-CM. In this case

$$Q(s;\hat{\boldsymbol{k}}) = s + k_3 + k_4 \tag{64}$$

and

$$D(s;\hat{\boldsymbol{k}}) = s^2 + (k_2 + k_3 + k_4)s + k_2 k_4\,, \tag{65}$$

which do not have any common roots and have leading coefficient equal to 1. In this case, the necessary conditions in equation (63) lead to the system

$$\begin{cases} k_3 + k_4 = h_3 + h_4 \\ k_2 + k_3 + k_4 = h_2 + h_3 + h_4 \\ k_2 k_4 = h_2 h_4 \end{cases} \tag{66}$$

that straightforwardly implies $\hat{\boldsymbol{k}} = \hat{\boldsymbol{h}}$.

Some additional results on the identifiability of 2-CMs and 3-CMs can be found in [8] where also more general models are consider, including, e.g., multiple compartments exchanging tracer with blood.

5.2. Sensitivity analysis

In the previous section we have shown how to analytically prove the identifiability of the rate constants of a linear CM. However, in practical scenarios, this analytic result does not guarantee that the rate constants may be effectively and reliably estimated. This may occur when changes in one or more parameters only slightly affect the data. For this reason, a local (or global) sensitivity analysis needs to be performed to investigate to what extent the state of the system changes when parameter values are perturbed from a reference value [15,16,39].

While for standard 2-CMs local sensitivity analysis shows that perturbations of the rate constants significantly affect the system variables, the 3-CM show a poor sensitivity with respect to k_5 and k_6 [49]. As a consequence, even though the parameters are identifiable, multiple configurations exist that equally fit the noisy recorded data. The uniqueness of the solution of the inverse problem can be restored by incorporating in the optimization procedure prior information on biologically feasible interval for the values of such parameters [49].

6. Physiology-driven compartmental models

CMs provide a highly flexible instrument which may be adapted to the analysis of tracer kinetics in non standard conditions. We examine here a few examples, focusing on the essential features of each approach. Each example accounts for a set of specific conditions and available PET data, which in turn suggest the most convenient approach to the modelling of tracer kinetics.

6.1. Reference tissue models

In the present formulation, reference tissue models (RTMs) result from the combination of 1-CM, 2-CM, and a graphical approach. RTMs have been introduced to overcome difficulties in the reconstruction of the TAC of the IF. Often, the IF is determined by measurements of activity on a ROI which is drawn over a sufficiently large blood pool, such as the left ventricle, but the procedure is subject to systematic errors. Possible sources of error are given by spillover, cardiac motion, and the low resolution of PET cameras (see [52] and the related references). Moreover, at the very beginning of the diffusion process the arterial TAC shows a very high peak, which is difficult to estimate reliably [43]. The essential idea of RTMs, is that the TAC of a suitably chosen reference tissue (RT) replaces the TAC of the IF of the target tissue.

We consider an RTM which is formed by a reversible 2-CM for the TT, and a 1-CM for the RT, as shown in figure 1. In particular, C_R denotes tracer concentration in the RT, while k_{1R} and k_{2R} [min^{-1}] are the rate constants for incoming tracer flow from blood, and outgoing flow to blood, respectively. Thus, the RTM depends on six unknown kinetic parameters. The natural data are the time dependent radioactivity concentration $\mathcal{C}_R$ of the RT, and total concentration $\mathcal{C}_T$ of the target tissue (TT). In the present formulation we also assume that the concentration C_b of blood is known from t_0 on, with t_0 sufficiently large. We show that the IPE for the unknown rate constants may be formulated in terms of these data.

Following the approach of [43] we describe first the RT. The concentration C_R solves the Cauchy problem for the 1-CM:

$$\dot{C}_R = -k_{2R}\, C_R + k_{1R}\, C_b, \qquad C_R(0) = 0\,. \tag{67}$$

We denote by V_{bR} the given volume fraction of RT. Then the measured total radioactivity concentration $\mathcal{C}_R$ is expressed as

$$\mathcal{C}_R = (1 - V_{bR})\, C_R + V_{bR}\, C_b. \tag{68}$$

As to the TT, this is represented as a 2-CM. Hence equation (29) applies, with $\boldsymbol{M}$, $\boldsymbol{C}$, and $\boldsymbol{e}$ given by (30). It follows that

$$\boldsymbol{C} = k_1 \int_0^t e^{\boldsymbol{M}\,(t-\tau)}\;\; C_b(\tau)\, d\tau\, \boldsymbol{e}\,, \tag{69}$$

where the unknown parameters are (k_1, k_2, k_3, k_4). Notice that equation (69) is a particular case of the general representation (32), which has been restated here for convenience. The connection between the measured total radioactivity concentration $\mathcal{C}_T$ of the TT and the related state vector $\boldsymbol{C}$ of equation (69) follows from equation (33), which here takes the form

$$\mathcal{C}_T = \boldsymbol{\alpha}_T\, \boldsymbol{C} + V_{bT}\, C_b, \qquad \boldsymbol{\alpha}_T = (1 - V_{bT})\,\begin{bmatrix}1 & 1\end{bmatrix}, \tag{70}$$

where V_{bT} is the given volume fraction of the TT.

In order to find the IPE for the RTM we proceed according to three steps.

In the first step the constant k_{2R} is expressed in terms of k_{1R} by the use of RT data. This reduces the number of the unknown parameters from 6 to 5, and guarantees the identifiability. Specifically, we set

$$k_{2R} = \lambda\, k_{1R}, \tag{71}$$

where λ is a constant unknown parameter that may be estimated by a graphical approach. Indeed, it follows from (67) and (68) that the following identity holds:

$$\frac{\int_{t_0}^t \mathcal{C}_R}{\mathcal{C}_R} = \gamma_1 \frac{\int_{t_0}^t C_b}{\mathcal{C}_R}, + \gamma_2(t)\,, \tag{72}$$

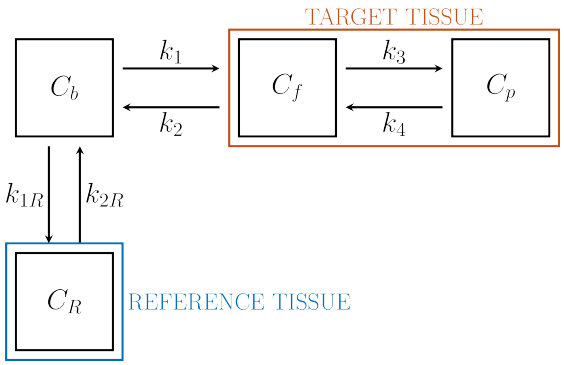

Figure 1. Compartment model for the reference tissue.

where

$$\gamma_1 = \frac{1 - V_{bR}}{\lambda} + V_{bR}.$$

Under the assumption that γ_2 is asymptotically constant equation (72) provides γ_1 by linear regression, and hence λ.

In the second step C_b is expressed in terms of $\mathcal{C}_R$ as a consequence of equations (67) and (68) for the RT. It is found that

$$C_b = \frac{\mathcal{C}_R}{V_{bR}} - (V_{bR}^{-1} - 1)\, k_{1R} \int_0^t e^{-\gamma k_{1R}(t-\tau)}\, \mathcal{C}_R\, d\tau\,. \tag{73}$$

In the third step, replacement of C_b in (69) with its expression (73) yields the state vector $\boldsymbol{C}$ in terms of $\mathcal{C}_R$. Subsequent substitution of $\boldsymbol{C}$ and C_b in (70) provides the IPE for the five unknowns $k_{1R}, k_1, k_2, k_3, k_4$.

Identifiability is proved by considering the Laplace transforms of equations (29) and (70). The details can be found in [43].

We conclude this section with a few remarks. The volume fraction V_{bR} and V_{bT} are often set equal to zero. The number of the unknown parameters is reduced by the assumption that the distribution volumes of tracer of the two tissues are equal; this corresponds to imposing

$$\frac{k_1}{k_2} = \frac{k_{1R}}{k_{2R}}$$

but application of this the assumption to tumor tissues has been subject to criticism. We refer again to [43] for more details.

6.2. CMs for liver

In applications of compartmental analysis to the liver system there are two input functions to consider in that blood, and hence the tracer is supplied to liver by both the hepatic artery (HA) and the portal vein (PV), which carries to the liver the blood outgoing from the gut. While tracer concentration in HA may be estimated by the methods developed for standard IFs, the PV is not accessible to PET images. As observed in [12], there have been several attempts to estimate the dual-input IFs from dynamic PET data. According to the approach of [12], a reliable solution is provided by combination of three compartmental models and suitable physiologic remarks.

As described in Figure 2, we developed a compartmental approach resulting from the combination of two 2-CM subsystems for tracer kinetics in the gut and the liver, respectively, and a 1-CM subsystem for the portal vein, regarded as a pool connecting gut and liver.

The gut subsystem is regarded as a reversible 2-CM with arterial blood concentration for IF, and portal vein concentration for the output function. The following system of ODEs holds, which is simply a restatement of the ODEs for a 2-CM:

$$\dot{C}'_f = -(k'_{vf} + k'_{pf})\, C'_f + k'_{fp}\, C'_p + k'_{fb}\, C_b \tag{74}$$
$$\dot{C}'_p = k'_{pf}\, C'_f - k'_{fp}\, C'_p\,. \tag{75}$$

Here C'_f and C'_p denote the tracer concentrations of the free compartment $\mathcal{C}'_f$, and the phosphorylated compartment $\mathcal{C}'_p$, respectively; C_b is the arterial blood concentration. We remark that the notation for the rate coefficients has been changed in order to take into account the complicated structure of the model: specifically, k_{ij} denotes the rate coefficient for tracer transfer to the target compartment $\mathcal{C}_i$ from the source compartment $\mathcal{C}_j$. In particular, k'_{vf} is related to the rate of transfer to the PV from gut.

The total concentration $C_{T,\text{gut}}$ of the gut system and the IF C_b are accessible to measurement and hence are regarded as data for the standard compartmental problem. Thus the rate coefficients are determined by solving the IPE

$$C_{T,\text{gut}} = C'_f + C'_p,$$

where a vanishing blood volume fraction is considered. The coefficients are replaced into the system (74), (75), so that the concentrations C'_f and C'_p are evaluated by solving the related Cauchy problem with vanishing initial data. In particular, the time course of C'_f is required for further developments.

The PV subsystem, denoted as $\mathcal{C}_v$, provides the input concentration to liver from gut. Tracer carried by blood leaves the free gut compartment $\mathcal{C}'_f$, goes through $\mathcal{C}_v$, and enters the free liver compartment $\mathcal{C}_f$. While observing that the incoming and the outgoing blood flows of $\mathcal{C}_v$ are constant, it is found that $k'_{vf} = k_{fv}$. Thus the ODE for the concentration C_v takes the form

$$\dot{C}_v = k'_{vf} C_f - k'_{vf} C_v;$$

its formal solution yields the expression of C_v in terms of $C'_f(t)$ and the rate constant k'_{vf}.

The liver subsystem is modeled as a reversible 2-CM. The ODEs for the concentrations C_f and C_p, of free and metabolized compartments are

$$\dot{C}_f = -(k_{pf} + k_{sf})\, C_f + k_{fp}\, C_p + k_{fb}\, C_b + k'_{vf} C_v\,, \tag{76}$$
$$\dot{C}_p = k_{pf}\, C_f - k_{fp}\, C_p\,. \tag{77}$$

The interpretation of the rate coefficients follows according to the general rules, with the further remark that k_{sf} is the rate towards the suprahepatic vein from the liver free pool $\mathcal{C}_f$. The IFs C_b and C_v can now be regarded as given. The IPE takes the form

$$C_{T,\text{liver}} = (1 - V_b)\,(C_f + C_p) + V_b\,(0.11 C_b + 0.89 C_v),$$

where $C_{T,\text{liver}}$ is the measured concentration in liver, while the numerical coefficients 0.11 and 0.89 refer to the rate of arterial and venous contributions to the hepatic blood content V_b per unit volume. The unknowns are the 5 rate constants k_{pf}, k_{sf}, k_{fp}, k_{fb}, k'_{vf}.

6.3. CMs for the renal system

Tracer subtraction from blood by the renal system, besides being of interest in itself, may be influenced by the presence of drugs, thus leading to possible therapeutic applications [11]. A quantitative analysis of the process of renal excretion involves a compartment anatomically represented by the bladder, which is thus to be considered in the formulation of the renal CM. Moreover, the change of tracer concentration in tubules associated with

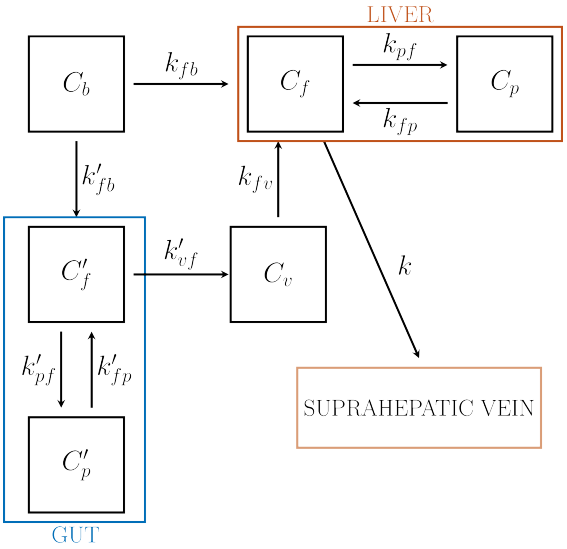

Figure 2. Compartment model for liver.

re-absorption of liquid must also be considered. Insertion of these conditions makes the CM of the renal system rather complex.

A concise description of models available in the literature can be found in [11,13]. Here we describe the CM of [11], which is capable of accounting for a number of physiological conditions.

We refer to Figure 3, showing that the renal CM involves four compartments, which can be given the following interpretations:

- An extravascular compartment $\mathcal{C}_f$ accounting for tracer outside cells, whose exchange with blood is free.
- A compartment $\mathcal{C}_p$ containing the phosphorylated FDG, the FDG in the cells and the preurine pool. In particular, following the flow of liquid, tracer is filtered in the preurines and carried towards the proximal tubule. This compartment, has been denoted as $\mathcal{C}_p$ because tracer can also be in phosphorylated form.
- A tubular compartment $\mathcal{C}_t$, where tracer flows towards bladder. Here the concentration varies (increases) because of the re-absorption of liquids through the tubular walls.
- The urinary pool $\mathcal{C}_u$, anatomically identified with the bladder, where the tracer carried by the urine is accumulated. Notice the bladder volume varies with time.

Following the standard conventions, the system of ODEs may be written as follows:

$$\dot{C}_f = -(k_{bf} + k_{pf})\, C_f + k_{fp}\, C_p + k_{fb}\, C_b\,, \tag{78}$$

$$\dot{C}_p = k_{pf}\, C_f - (k_{fp} + k_{tp})\, C_p + k_{pb} C_b, \tag{79}$$

$$\dot{C}_t = -k_{ut}\, C_t + k_{tp} C_p, \tag{80}$$

and

$$\frac{d}{dt}(V_u C_u) = F_{ut} C_t. \tag{81}$$

Notice that V_u denotes the time dependent volume of the bladder, so that $V_u C_u$ is the corresponding total activity content. F_{ut} (ml min^{-1}) denotes the bulk flow of urine from tubules to bladder; according to the assumption of stationarity, F_{ut} is considered constant.

The total radioactivity C_K of the kidneys may be written as

$$C_K = (1 - \eta_b - \eta_t)(C_f + C_p) + \eta_t C_t + \eta_b C_b, \tag{82}$$

where η_b and η_t denote the fractions of kidney volume V_K occupied by the tubular compartment and the blood compartment, respectively; they are regarded as given. The measured data are C_K, C_u, and V_u.

A rather complicated formal development (see [11]) shows that, in view of (78)-(80), equations (82) and (81) are approximated by

$$A_K = x_1 V_K C_b + x_2 \int_0^t A_K + x_3 V_K \int_0^t C_b + x_4 V_K A_u, \tag{83}$$

$$A_u = z_1 \int_0^t \int_0^\tau C_k + z_2 \int_0^t \int_0^\tau C_b + z_3 \int_0^t A_u. \tag{84}$$

Here $A_K = V_K C_K$ and $A_u = V_u C_u$ represent the total activities of kidneys and bladder, respectively. They are considered as given, since they are expressed in terms of given data. The parameters (x_1, x_2, x_3, x_4) and (z_1, z_2, z_3) depend on the rate constants k_{ij}, the volume fractions η_b and η_t, and the flow parameter F_{ut}. System (83), (84) provides the starting point for the solution of the inverse problem for the unknown rate constants.

The number of unknowns is reduced by the introduction of two physiological constraints.

First, the constant flux rate F_{ut} into bladder can be estimated from the measured bladder volumes as

$$F_{ut} = \frac{V_u(t_f) - V_u(t^*)}{t_t - t^*}$$

where t_f is the final time, and t^* is any intermediate time.

Second, we recall that the bulk flow of carrier fluid from $\mathcal{C}_t$ toward the bladder is around two orders of magnitude smaller than the reabsorbed flow through the boundary of $\mathcal{C}_t$. Therefore, the tracer balance equation in tubule implies $k_{tp} = 10^2 k_{ut}$. Finally, it follows from the definitions that $k_{ut}\, \eta_t V_K = F_{ut}$, whence k_{ut} and k_{tp} follow.

A simplified version of this renal system proposed in [13] provides an example of application of an inversion procedure inspired by biology. Here the bladder volume has been regarded as constant, while the compartment $\mathcal{C}_t$, which accounts for the presence of water re-absorption in tubule, has not been considered.

The ODEs of the simplified model take the form

$$\dot{C}_f = -(k_{bf} + k_{pf})\, C_f + k_{fp}\, C_p + k_{fb}\, C_b, \tag{85}$$

$$\dot{C}_p = k_{pf}\, C_f - (k_{fp} + k_{up})\, C_p + k_{pb} C_b, \tag{86}$$

$$\dot{C}_u = k_{up} C_p. \tag{87}$$

The formal expressions of $C_f(t)$ and $C_p(t)$ are obtained by solving the Cauchy Problem (85), (86) with vanishing initial conditions. Then, $C_u(t)$ is determined by integration in time of $k_{up} C_p$. The data are the total renal concentration C_K, the bladder concentration $\bar{C}_u$, and the IF C_p. The total renal concentration C_K is related to the unknown rates by the equation

$$C_K = (1 - V_b)(C_f + C_p) + V_b C_b \tag{88}$$

while $\bar{C}_u$ and C_u are simply related by $\bar{C}_u = \bar{C}_u$.

6.4. The role of the endoplasmic reticulum

In Subsection 3.3.3 we have discussed a three-compartment model that aims to account for the crucial role played by the endoplasmic reticulum in cancer FDG metabolism. This model relies on results obtained by means of an *in vitro* argument [44] and has been recently confirmed *in vivo* using data recorded by means of a PET device for animal models [49]. A scheme of the model is illustrated in Figure 4 and the corresponding equations have been discussed in Subsection 3.3.3.

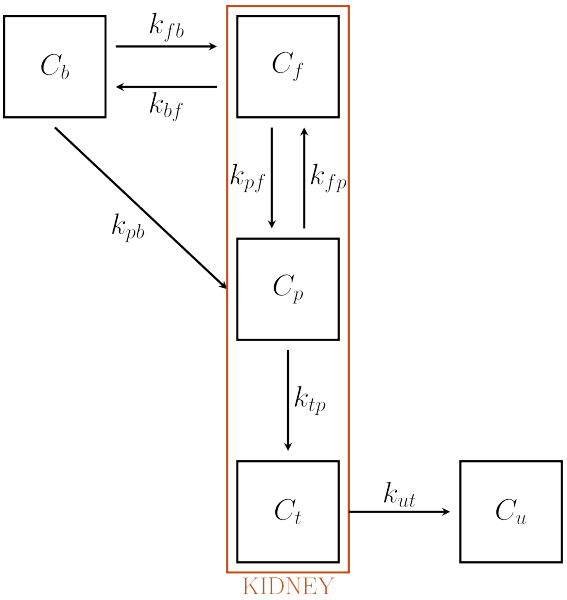

Figure 3. Compartment model for the renal system

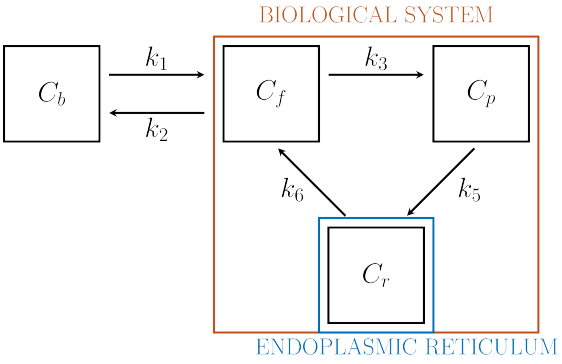

Figure 4. Compartment model for cell absorption

7. Some numerics: optimization schemes

The way compartmental analysis can be actually exploited for modelling the tracer kinetics in nuclear medicine relies on the numerical solution of the IPE equation (33). In experimental applications, the input data is given by the time series $C_T = C_T(t)$, which is determined by computing the pixel content in Regions of Interest (ROIs) of the reconstructed PET data at different time points; $C_b = C_b(t)$ is the input function, which is also determined from PET data; and the unknown is represented by the vector $\boldsymbol{k}$ whose components are the tracer coefficients, and by V_b. By denoting the right hand side of equation (33) as

$$\mathcal{F}(\boldsymbol{k}, V_b) := \boldsymbol{\alpha}\, \boldsymbol{C}(t; \boldsymbol{k}, C_b) + V_b\, C_b, \tag{89}$$

the computational problem of compartmental analysis is therefore the one to determine, at each time point,

$$(\boldsymbol{k}^*, V_b^*) = \arg\min_{\boldsymbol{k}, V_b} \|C_T - \mathcal{F}(\boldsymbol{k}, V_b)\| \,. \tag{90}$$

In this optimization equation, $\|\cdot\|$ denotes the topology with which the distance between the experimental and predicted total concentrations is measured. Naive approaches to the computational solution of equation (90) are typically characterized by three main drawbacks:

- They typically suffer numerical instabilities related to the non-uniqueness and sensitivity limitations discussed in Section 5.
- Since the operator $\mathcal{F}$ is clearly non linear and, further, the space where possible minimizers can be searched for is typically big, they may suffer local minima.
- Particularly in the case of three-compartment models, the number of kinetic parameters to determine is high, which implies that they are computationally demanding.

Several numerical methods have been applied for the solution of equation (90), whose reliability and computational effectiveness depend on the choice of the topology $\|\cdot\|$ and by the way possible prior information on the solution are encoded in the optimization process. Further, the computational algorithms utilized for solving the minimization problem typically belong to three general approaches: the deterministic, statistical, and biology-inspired ones. In the following we will provide a sketch of the main computational aspects of these three approaches, assuming that V_b is known thanks to either experimental or physiological information (the generalization to the case when also V_b is an unknown parameter is straightforward).

7.1. Deterministic approaches

Most deterministic approaches utilize numerical methods to solve the minimum problem [18]

$$\boldsymbol{k}^* = \arg\min_{\boldsymbol{k}, V_b} \{\|C_T - \mathcal{F}(\boldsymbol{k})\|_2 + \lambda \|\boldsymbol{k}\|_p^p\} \,, \tag{91}$$

where λ is the so called regularization parameter tuning the trade-off between the fitting capability of the algorithm and its numerical stability. The least-squares problem corresponding to $\lambda = 0$ is often addressed either by means of the standard Levenberg-Marquardt scheme [20] or by using generalized separable parameter space techniques [21,59]. Other deterministic methods re-formulate the compartmental problem as the non-linear zero-finding problem

$$F_T = 0 \,, \tag{92}$$

with

$$F_T := C_T - \mathcal{F}(\boldsymbol{k}) \tag{93}$$

and apply an iterative Gauss-Newton approach for its solution [44,45]. Finally, more recently a regularized affine-scaling trust-region optimization methods has been introduced to solve the compartmental method in a rapid fashion, so that applications to parametric imaging are possible and computationally effective [9].

7.2. Statistical approaches

The general framework where statistical approaches are formulated is the Bayes theorem, which, in this context, can be written as

$$\pi(\boldsymbol{k}|C_T) = \frac{\pi(C_T|\boldsymbol{k})\pi(\boldsymbol{k})}{\pi(C_T)} \,. \tag{94}$$

In this equation $\pi(C_T|\boldsymbol{k})$ is the likelihood distribution depending on $\mathcal{F}$ and on the statistical properties of the noise affecting the measurements (which is Poissonian); $\pi(\boldsymbol{k})$ is the prior distribution encoding all the *a priori* information at disposal on the solution; $\pi(C_T)$ is a normalization factor. The posterior distribution $\pi(\boldsymbol{k}|C_T)$ is the solution of the compartmental inverse problem, which can be utilized to compute $\boldsymbol{k}$ via either the maximum a posteriori

$$\boldsymbol{k}_{map} = \arg\max_{k} \pi(\boldsymbol{k}|C_T) \,, \tag{95}$$

or the conditional mean

$$\boldsymbol{k}_{CM} = \int \pi(\boldsymbol{k}|C_T) dC_T \,. \tag{96}$$

If the prior distribution is just concerned with the positivity of the solution, it is well-established that $\boldsymbol{k}_{map}$ can be determined by means of the expectation maximization iterative scheme [5,11,50]. Encoding more sophisticated prior information in the Bayesian framework requires the implementation of more sophisticated Monte Carlo schemes for the computation of the posterior distribution [4,22,29,37,60,61].

7.3. Biology-inspired approaches

Some recent approaches to the computational solution of tracer kinetics problems exploit optimization schemes that rely on biological inspiration. An example of how this perspective may be helpful in compartmental analysis is illustrated in [13], where an optimization scheme inspired by ant colony behavior is utilized to determine the kinetic parameters. However, most optimization algorithms belonging to this group of methods rely on neural networks that are formulated within the framework of machine and deep learning theory [24,35,57]

In order to show how some of these methods behave in action, Figure 5 summarizes some results obtained in the literature by using experimental measurements recorded by means of a PET scanner for small animals. TThese results refer to the four CMs discussed in Section 6. Specifically, in this figure the parameter values obtained in panel A refer to the reference tissue model in Figure 1 and have been obtained by means of a deterministic Gauss-Newton scheme [43]. An analogous deterministic algorithm has been utilized in panel B [12] to compute the parameter of the liver physiology illustrated in Figure 2. Panel C and Panel D refer to the renal physiology modelled in Figure 3 and the parameters have been computed by means the biology inspired Ant Colony Optimization algorithm [13] and by the statistical Expectation Maximization iterative scheme [11], respectively. Finally, panel E contains the tracer parameters provided by a regularized Gauss-Newton method [49] in the case of the model including the endoplasmic reticulum illustrated in Figure 4. Just a few comments on these results: most standard errors are rather small, which shows the stability effects related to the introduction of regularization in the optimization process; the small value of k_{pf} in panel B confirms the fact that metformin leave this parameter essentially unaltered (indeed, these results have been obtained in the case of six tumor models treated with metformin); panel C and panel D show the effect of metformin on k_{bf}; panel E shows that the analogous parameter for the model accounting for the role of the endoplasmic reticulum (i.e., k_2) significantly decreases with respect to the case when the reticulum is neglected.

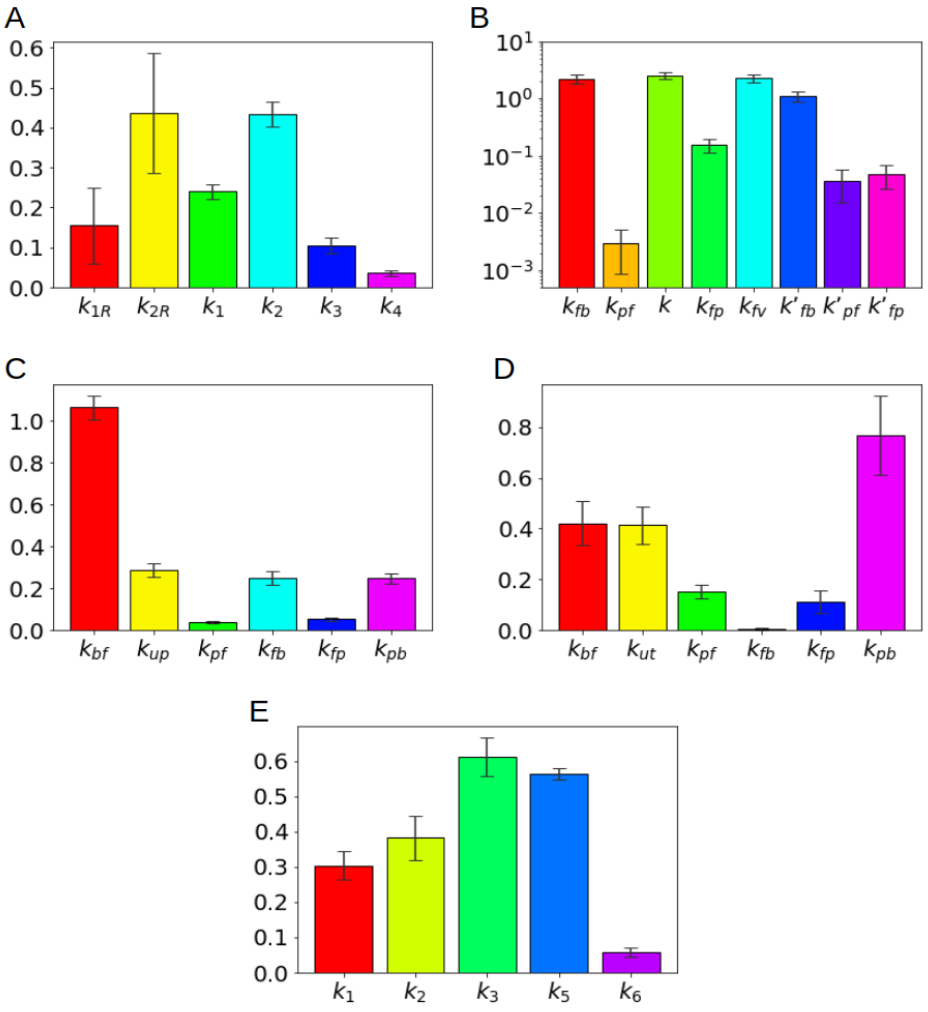

Figure 5. (A) Kinetic parameters estimated for the reference tissue CM with a deterministic approach (B) Kinetic parameters estimated for the liver CM with a deterministic approach (C) Kinetic parameters for a simplified CM for the renal system estimated with ant colony optimization, (D) Kinetic parameters for the CM of the renal system estimated with a statistical approach (D) Kinetic parameters of the CM including the endoplasmic reticulum estimated with a regularized Gauss-Newton approach.

8. Conclusions

Compartmental analysis is a well-established approach to the interpretation of dynamical FDG-PET data and this review paper has aimed to point out the fact that numerical algorithms for the reduction of compartmental models play a crucial role for the comprehension of cancer glucose metabolism from a quantitative viewpoint. Yet, some technical issues are still open, whose solution would imply a further significant improvement in the comprehension of glucose dynamics in cancerous tissues.

First, the approaches illustrated in this review all rely on an indirect perspective, in which the compartmental analysis is performed on the reconstructed PET images. However, direct parametric imaging [23, 46] can be realized by using as input the raw PET sinograms and then by solving the inverse problem relating the kinetic parameters to such sinograms. These one-shot approaches are not currently employed for the systematic analysis of FDG-PET data, mainly because they would have to account for the intertwining of temporal and spatial correlations, which might increase the complexity of the optimization process. However, they certainly present significant potential advantages, since they may exploit the use of input data characterized by a well-established statistical distribution and a higher signal-to-noise ratio.

Second, image processing could improve the numerical solution of the compartmental equations by introducing morphological information that can be exploited in the computation of the total concentration. More specifically, a possible scheme would rely on a segmentation step applied on the co-registered CT image that automatically identify the voxels corresponding to the organ (namely, the tumor) and by the generation of a binary map that is multiplied against the FDG-PET reconstructed map in order to allow an accurate computation of the total concentration.

Finally, all methods described in this review explicitly assume that the tracer concentration in blood at the beginning of the compartmental experiment is zero. This is reflected into a vanishing initial condition in the Cauchy problem that significantly simplifies the computation. However, in clinical applications the initial concentration is not zero and a significant improvement of the reliability of the compartmental models would be gained by dealing with a non-vanishing Cauchy condition as a further unknown in the differential problem.

Appendix

We show the main steps of the procedure leading to eq (34) for the Patlak plot. Consider an irreversible CM with n compartments, and suppose that $\mathcal{C}_n$ is the irreversible compartment where accumulation of tracer occurs. In principle, C_n acquires tracer from $\mathcal{C}_1$, ... $\mathcal{C}_{n-1}$ with rates h_1, ..., h_{n-1}; no compartment receives tracer from $\mathcal{C}_n$. As in the rest of the paper, $\mathcal{C}_1$ is the compartment which exchanges tracer with the exterior environment.

The original n-dimensional system (29) is decomposed into a reduced $(n-1)$-dimensional system for $\hat{\boldsymbol{C}} = [C_1, \ldots, C_{n-1}]^T$ and a single differential equation for C_n. To this aim, denote as $\boldsymbol{h}$ the $n-1$ row vector of components h_1, ... , h_{n-1} and consider the block decomposition

$$\boldsymbol{M} = \begin{bmatrix} \hat{\boldsymbol{M}} & \boldsymbol{0} \\ \boldsymbol{h} & 0 \end{bmatrix}, \quad \boldsymbol{C} = \begin{bmatrix} \hat{\boldsymbol{C}} \\ C_n \end{bmatrix}, \tag{A97}$$

where $\hat{\boldsymbol{M}}$ is a non-singular square matrix of order $n-1$, and $\boldsymbol{0}$ is the $(n-1)$-column vector of vanishing components. The system (29) is equivalent to the ODEs

$$\frac{d\hat{\boldsymbol{C}}}{dt} = \hat{\boldsymbol{M}}\,\hat{\boldsymbol{C}} + k_1\, C_b\, \hat{\boldsymbol{e}},$$

$$\dot{C}_n = \boldsymbol{h}\,\hat{\boldsymbol{C}},$$

where $\hat{\boldsymbol{e}}$ is the $(n-1)$-column vector of vanishing components with exception of the first, of value 1.

It is found by integration of the two differential equations that

$$\hat{\boldsymbol{C}} = k_1 \int_0^t e^{\hat{\boldsymbol{M}}\,(t-\tau)}\; C_b(\tau)\, d\tau\, \hat{\boldsymbol{e}}, \tag{A98}$$

$$C_n = \boldsymbol{h} \int_0^t \hat{\boldsymbol{C}}(\sigma)\, d\sigma. \tag{A99}$$

Substitution of (A98) into (A99) leads to

$$C_n = \boldsymbol{h} \int_0^t k_1 \int_0^\sigma e^{\hat{\boldsymbol{M}}\,(\sigma-\tau)}\; C_b(\tau)\, d\tau\, d\sigma\, \hat{\boldsymbol{e}}.$$

Partial integration provides an alternative expression of C_n as

$$C_n = \boldsymbol{h}\, \hat{\boldsymbol{M}}^{-1} \left[k_1 \int_0^t e^{\hat{\boldsymbol{M}}\,(t-\tau)}\, C_b(\tau)\, d\tau - k_1 \int_0^t C_b(\tau)\, d\tau \right] \hat{\boldsymbol{e}} \tag{A100}$$

The vector $\boldsymbol{C} = [\hat{\boldsymbol{C}}, C_n]^T$ is recovered by substitution of (A98) and (A100). Further insertion of $\boldsymbol{C}$ into the IPE (33) and division by C_b leads to eq (34). Precisely, consider eq (33) in the form

$$C_T = \hat{\boldsymbol{\alpha}} \hat{\boldsymbol{C}} + \alpha_n\, C_n + V_b\, C_b,$$

where $\boldsymbol{\alpha}$ has been decomposed according as $\boldsymbol{\alpha} = [\hat{\boldsymbol{\alpha}}, \alpha_n]$. Division by C_b and substitution of C_n leads to

$$\frac{C_T}{C_b} = -\alpha_n\, \boldsymbol{h}\, \hat{\boldsymbol{M}}^{-1}\, \hat{\boldsymbol{e}}\, k_1\, \frac{\int_0^t C_b}{C_b} + \alpha_n\, \boldsymbol{h}\, \hat{\boldsymbol{M}}^{-1}\, k_1\, \frac{\int_0^t e^{\hat{\boldsymbol{M}}\,(t-\tau)}\, C_b(\tau)\, d\tau}{C_b}\, \hat{\boldsymbol{e}} + \hat{\boldsymbol{\alpha}}\, \frac{\hat{\boldsymbol{C}}}{C_b} + V_b$$

that is,

$$\frac{C_T}{C_b} = \alpha_P\, \frac{\int_0^t C_b}{C_b} + \beta_P(t),$$

where, in particular,

$$\alpha_P = -\alpha_n\, \boldsymbol{h}\, \hat{\boldsymbol{M}}^{-1}\, \hat{\boldsymbol{e}}\, k_1.$$

For example, in the case of a 3-CM the expression of α_P reduces to the form (43), as expected.

To find the interpretation of α_P, consider the case of a constant IF C_b^*. The corresponding equilibrium value of $\hat{\boldsymbol{C}}$ is given by

$$\hat{\boldsymbol{C}}^* = -k_1\, \hat{\boldsymbol{M}}^{-1} \hat{\boldsymbol{e}}\, C_b^*.$$

Substitution shows that the rate $\dot{C}_n$ is constant and is expressed as

$$\dot{C}_n^* = \boldsymbol{h}\, \hat{\boldsymbol{C}}^* = -k_1\, \boldsymbol{h}\, \hat{\boldsymbol{M}}^{-1} \hat{\boldsymbol{e}}\, C_b^*$$

Finally, evaluation of the time derivative of (33) under the above conditions shows that

$$\dot{C}_T^* = \alpha_n\, \dot{C}_n^* = -\alpha_n\, k_1\, \boldsymbol{h}\, \hat{\boldsymbol{M}}^{-1} \hat{\boldsymbol{e}}\, C_b^* = \alpha_P\, C_b^*$$

We conclude that α_P represents the rate of tracer accumulation at constant IF, namely, $\alpha_P = \dot{C}_T^* / C_b^*$.

Author Contributions: Conceptualization, S.S., G.C., G.S. and M.P.; methodology, S.S., G.C. and M. P; software, not applicable; validation, not applicable; formal analysis, not applicable; investigation, S.S., G.C., G.S. and M.P.; resources, not applicable; data curation, not applicable; writing—original draft preparation, S.S., G.C. and M.P.; writing—review and editing, S.S., G.C. and M.P.; visualization, S.S.; supervision, G.C., G.S. and M.P; project administration, G.S. and M.P; funding acquisition, G.S. and M.P.; all authors have read and agreed to the published version of the manuscript.

Funding: This research was funded by the Italian AIRC, grant number IG 230201.

Institutional Review Board Statement: This is a review paper that has not required any approval from our Institutional Review Board.

Informed Consent Statement: Not applicable

Data Availability Statement: Not applicable

Acknowledgments: The Italian AIRC grant number IG 230201, is kindly acknowledged.

Conflicts of Interest: The authors declare no conflict of interest.

References

1. Adams, M.C.; Turkington, T.G.; Wilson, J.M.; Wong, T.Z. A systematic review of the factors affecting accuracy of SUV measurements. *AJR Am. J. Roentgenol.* **2010**, *195*, 310–320.
2. Bertoldo, A.; Rizzo, G.; Veronese, M. Deriving physiological information from PET images: from SUV to compartmental modelling. *Clin. Transl. Imaging* **2014**, *2*, 239–251.
3. Büsing, K.A.; Schönberg, S.O.; Brade, J.; Wasser, K. Impact of blood glucose, diabetes, insulin, and obesity on standardized uptake values in tumors and healthy organs on 18F-FDG PET/CT. *Nucl. Med. Biol.* **2013**, *40*, 206–213.
4. Castellaro, M.; Rizzo, G.; Tonietto, M.; Veronese, M.; Turkheimer, F.E.; Chappell, M.A.; Bertoldo, A. A Variational Bayesian inference method for parametric imaging of PET data. *NeuroImage* **2017**, *150*, 136–149.
5. Cheng, X.; Li, Z.; Liu, Z.; Navab, N.; Huang, S.C.; Keller, U.; Ziegler, S.I.; Shi, K. Direct parametric image reconstruction in reduced parameter space for rapid multi-tracer PET imaging. *IEEE Trans. Med. Imaging.* **2015**, *34*, 1498–1512.
6. Cherry, S.R.; Sorenson, J.A.; Phelps, M.E. *Physics in nuclear medicine*; Elsevier Health Sciences, 2012.
7. Chis, O.T.; Banga, J.R.; Balsa-Canto, E. Structural identifiability of systems biology models: a critical comparison of methods. *PloS one* **2011**, *6*, e27755.
8. Cobelli, C.; Foster, D.; Toffolo, G. *Tracer Kinetics in Biomedical Research*; Kluwer Academic Publishers New York, 2002.
9. Crisci, S.; Piana, M.; Ruggiero, V.; Scussolini, M. A Regularized Affine-Scaling Trust-Region Method for Parametric Imaging of Dynamic PET Data. *SIAM J. Imaging Sci.* **2021**, *14*, 418–439.
10. Csala, M.; Marcolongo, P.; Lizák, B.; Senesi, S.; Margittai, É.; Fulceri, R.; Magyar, J.É.; Benedetti, A.; Bánhegyi, G. Transport and transporters in the endoplasmic reticulum. *Biochim Biophys Acta Biomembr* **2007**, *1768*, 1325–1341.
11. Garbarino, S.; Caviglia, G.; Sambuceti, G.; Benvenuto, F.; Piana, M. A novel description of FDG excretion in the renal system: application to metformin-treated models. *Phys. Med. Biol.* **2014**, *59*, 2469.
12. Garbarino, S.; Vivaldi, V.; Delbary, F.; Caviglia, G.; Piana, M.; Marini, C.; Capitanio, S.; Calamia, I.; Buschiazzo, A.; Sambuceti, G. A new compartmental method for the analysis of liver FDG kinetics in small animal models. *EJNMMI Res.* **2015**, *5*, 35.
13. Garbarino, S.; Caviglia, G.; Brignone, M.; Massollo, M.; Sambuceti, G.; Piana, M. Estimate of FDG excretion by means of compartmental analysis and ant colony optimization of nuclear medicine data. *Comput. Math. Methods Med.* **2013**, *2013*.
14. Ghosh, A.; Shieh, J.J.; Pan, C.J.; Sun, M.S.; Chou, J.Y. The catalytic center of glucose-6-phosphatase. HIS176 is the nucleophile forming the phosphohistidine-enzyme intermediate during catalysis. *J. Biol. Chem.* **2002**, *277*, 32837–32842.
15. Gonnet, P.; Dimopoulos, S.; Widmer, L.; Stelling, J. A specialized ODE integrator for the efficient computation of parameter sensitivities. *BMC Syst. Biol.* **2012**, *6*, 1–13.
16. Goulet, D. Modeling, simulating, and parameter fitting of biochemical kinetic experiments. *SIAM Rev.* **2016**, *58*, 331–353.
17. Gunn, R.N.; Gunn, S.R.; Cunningham, V.J. Positron emission tomography compartmental models. *J. Cer. Blood Flow Metab.* **2001**, *21*, 635–652.
18. Gunn, R.N.; Gunn, S.R.; Turkheimer, F.E.; Aston, J.A.; Cunningham, V.J. Positron emission tomography compartmental models: a basis pursuit strategy for kinetic modeling. *J. Cer. Blood Flow. Metab.* **2002**, *22*, 1425–1439.
19. Hearon, J.Z. Theorems on linear systems. *Ann. NY Acad. Sci.* **1963**, *108*, 36–68.
20. Hong, Y.T.; Fryer, T.D. Kinetic modelling using basis functions derived from two-tissue compartmental models with a plasma input function: general principle and application to [18F] fluorodeoxyglucose positron emission tomography. *Neuroimage* **2010**, *51*, 164–172.
21. Kadrmas, D.J.; Oktay, M.B. Generalized separable parameter space techniques for fitting 1K-5K serial compartment models. *Nucl. Med. Phys.* **2013**, *40*, 072502.
22. Kamasak, M.E.; Bouman, C.A.; Morris, E.D.; Sauer, K. Direct reconstruction of kinetic parameter images from dynamic PET data. *IEEE Trans. Med. Imag.* **2005**, *24*, 636–650.
23. Kimura, Y.; Naganawa, M.; Shidahara, M.; Ikoma, Y.; Watabe, H. PET kinetic analysis—pitfalls and a solution for the Logan plot. *Ann. Nucl. Med.* **2007**, *21*, 1–8.
24. Kuttner, S.; Wickstrøm, K.K.; Lubberink, M.; Tolf, A.; Burman, J.; Sundset, R.; Jenssen, R.; Appel, L.; Axelsson, J. Cerebral blood flow measurements with ^{15}O-water PET using a non-invasive machine-learning-derived arterial input function. *J. Cereb. Blood Flow Metab.* **2021**, p. 0271678X21991393.
25. Lawson, R.S. Application of mathematical methods in dynamic nuclear medicine studies. *Phys. Med. Biol.* **1999**, *44*, R57–R98.

26. Liberti, M.V.; Locasale, J.W. The Warburg effect: how does it benefit cancer cells? *Trends Biochem. Sci.* **2016**, *41*, 211–218.
27. Logan, J.; Fowler, J.S.; Volkow, N.D.; Wolf, A.P.; Dewey, S.L.; Schlyer, D.J.; MacGregor, R.R.; Hitzemann, R.; Bendriem, B.; Gatley, S.J.; others. Graphical analysis of reversible radioligand binding from time–activity measurements applied to [N-^{11}C-methyl]-(–)-cocaine PET studies in human subjects. *J. Cereb. Blood Flow Metab.* **1990**, *10*, 740–747.
28. Maddalena, F.; Lettini, G.; Gallicchio, R.; Sisinni, L.; Simeon, V.; Nardelli, A.; Venetucci, A.A.; Storto, G.; Landriscina, M. Evaluation of glucose uptake in normal and cancer cell lines by positron emission tomography. *Mol. Imag.* **2015**, *14*, 7290–2015.
29. Malave, P.; Sitek, A. Bayesian analysis of a one-compartment kinetic model used in medical imaging. *J. Appl. Stat.* **2015**, *42*, 98–113.
30. Marini, C.; Ravera, S.; Buschiazzo, A.; Bianchi, G.; Orengo, A.M.; Bruno, S.; Bottoni, G.; Emionite, L.; Pastorino, F.; Monteverde, E.; others. Discovery of a novel glucose metabolism in cancer: The role of endoplasmic reticulum beyond glycolysis and pentose phosphate shunt. *Sci. Rep.* **2016**, *6*, 1–13.
31. Munk, O.L.; Keiding, S.; Baker, C.; Bass, L. A microvascular compartment model validated using ^{11}C-methylglucose liver PET in pigs. *Phys. Med. Biol.* **2017**, *63*, 015032.
32. Muzi, M.; Freeman, S.D.; Burrows, R.C.; Wiseman, R.W.; Link, J.M.; Krohn, K.A.; Graham, M.M.; Spence, A.M. Kinetic characterization of hexokinase isoenzymes from glioma cells: implications for FDG imaging of human brain tumors. *Nucl. Med. Biol.* **2001**, *28*, 107–116.
33. Ollinger, J.M.; Fessler, J.A. Positron-emission tomography. *IEEE Sign. Proc. Mag.* **1997**, *14*, 43–55.
34. Pacák, J.; Točík, Z.; Černỳ, M. Synthesis of 2-deoxy-2-fluoro-D-glucose. *J. Chem. Soc. D* **1969**, *2*, 77–77.
35. Pan, L.; Cheng, C.; Haberkorn, U.; Dimitrakopoulou-Strauss, A. Machine learning-based kinetic modeling: a robust and reproducible solution for quantitative analysis of dynamic PET data. *Phys. Med. Biol.* **2017**, *62*, 3566.
36. Patlak, C.S.; Blasberg, R.G.; Fenstermacher, J.D. Graphical evaluation of blood-to-brain transfer constants from multiple-time uptake data. *J. Cereb. Blood Flow Metab.* **1983**, *3*, 1–7.
37. Peng, J.Y.; Aston, J.A.; Gunn, R.N.; Liou, C.Y.; Ashburner, J. Dynamic positron emission tomography data-driven analysis using sparse Bayesian learning. *IEEE Trans. Med. Imag.* **2008**, *27*, 1356–1369.
38. Reske, S.N.; Kotzerke, J. FDG-PET for clinical use. *Eur. J. Nucl. Med.* **2001**, *28*, 1707–1723.
39. Saltelli, A.; Ratto, M.; Tarantola, S.; Campolongo, F. Sensitivity analysis for chemical models. *Chem. Rev.* **2005**, *105*, 2811–2828.
40. Schain, M.; Fazio, P.; Mrzljak, L.; Amini, N.; Al-Tawil, N.; Fitzer-Attas, C.; Bronzova, J.; Landwehrmeyer, B.; Sampaio, C.; Halldin, C.; others. Revisiting the Logan plot to account for non-negligible blood volume in brain tissue. *Eur. J. Nucl. Med. Mol. Imag. Res.* **2017**, *7*, 1–12.
41. Schmidt, K.C.; Turkheimer, F.E. Kinetic modeling in positron emission tomography. *Quart J Nucl med* **2002**, *46*, 70–85.
42. Schmidt, K. Which linear compartmental systems can be analyzed by spectral analysis of PET output data summed over all compartments? *J. Cereb. Blood Flow Metab.* **1999**, *19*, 560–569.
43. Scussolini, M.; Garbarino, S.; Piana, M.; Sambuceti, G.; Caviglia, G. Reference tissue models for FDG-PET data: Identifiability and solvability. *IEEE Trans. Rad. Plasma Med. Sci.* **2018**, *2*, 177–186.
44. Scussolini, M.; Bauckneht, M.; Cossu, V.; Bruno, S.; Orengo, A.M.; Piccioli, P.; Capitanio, S.; Yosifov, N.; Ravera, S.; Morbelli, S.; others. G6Pase location in the endoplasmic reticulum: implications on compartmental analysis of FDG uptake in cancer cells. *Sci. Rep.* **2019**, *9*, 1–14.
45. Scussolini, M.; Garbarino, S.; Sambuceti, G.; Caviglia, G.; Piana, M. A physiology-based parametric imaging method for FDG–PET data. *Inverse Probl.* **2017**, *33*, 125010.
46. Shaw, R.J. Glucose metabolism and cancer. *Curr. Opin. Cell Biol.* **2006**, *18*, 598–608.
47. Signorini, M.; Paulesua, E.; Friston, K.; Perani, D:; Colleluori A.; Lucignani, G.; Grassi, F; Bettinardi, V.; Frackowiak, R. S. J.; Fazio, F. Rapid assessment of regional cerebral metabolic abnormalities in single subjects with quantitative and nonquantitative [18F]FDG PET: A clinical validation of Statistical Parametric Mapping *Neuroimage* **1999**, *9*, -63–80.
48. Sokoloff, L.; Reivich, M.; Kennedy, C.; Rosiers, M.D.; Patlak, C.; Pettigrew, K.e.a.; Sakurada, O.; Shinohara, M. The [^{14}C]deoxyglucose method for the measurement of local cerebral glucose utilization: theory, procedure, and normal values in the conscious and anesthetized albino rat. *J. Neurochem.* **1977**, *28*, 897–916.
49. Sommariva, S.; Scussolini, M.; Cossu, V.; Marini, C.; Sambuceti, G.; Caviglia, G.; Piana, M. The role of endoplasmic reticulum in in vivo cancer FDG kinetics. *PloS one* **2021**, *16*, e0252422.
50. Szirmay-Kalos, L.; Kacsó, Á.; Magdics, M.; Tóth, B. Robust compartmental model fitting in direct emission tomography reconstruction. *Visu. Comput.* **2021**, pp. 1–14.
51. Vander Heiden, M.G.; Cantley, L.C.; Thompson, C.B. Understanding the Warburg effect: the metabolic requirements of cell proliferation. *Science* **2009**, *324*, 1029–1033.
52. Vriens, D.; de Geus-Oei, L.F.; Oyen, W.J.; Visser, E.P. A curve-fitting approach to estimate the arterial plasma input function for the assessment of glucose metabolic rate and response to treatment. *J. Nucl. Med.* **2009**, *50*, 1933–1939.
53. Warburg, O. The metabolism of carcinoma cells. *J. Cancer Res.* **1925**, *9*, 148–163.
54. Watabe, H.; Ikoma, Y.; Kimura, Y.; Naganawa, M.; Shidahara, M. PET kinetic analysis–compartmental model. *Ann. Nucl. Med.* **2006**, *20*, 583–588.
55. Wernick, M.N.; Aarsvold, J.N. *Emission tomography: the fundamentals of PET and SPECT*; Elsevier, 2004.

56. Williams, S.P.; Flores-Mercado, J.E.; Port, R.E.; Bengtsson, T. Quantitation of glucose uptake in tumors by dynamic FDG-PET has less glucose bias and lower variability when adjusted for partial saturation of glucose transport. *Eur. J. Nucl. Med. Mol. Imag. Research* **2012**, *2*, 1–13.
57. Xu, J.; Liu, H. Deep-learning-based separation of a mixture of dual-tracer single-acquisition PET signals with equal half-Lives: A simulation study. *IEEE Trans. Rad. Plasma Med. Sci.* **2019**, *3*, 649–659.
58. Zanotti-Fregonara, P.; Chen, K.; Liow, J.S.; Fujita, M.; Innis, R.B. Image-derived input function for brain PET studies: many challenges and few opportunities. *J. Cer. Blood Flow Metab.* **2011**, *31*, 1986–1998.
59. Zhang, J.L.; Morey, A.M.; Kadrmas, D.J. Application of separable parameter space techniques to multi-tracer PET compartment modeling. *Phys. Med. Biol.* **2016**, *61*, 1238.
60. Zhou, Y.; Aston, J.A.; Johansen, A.M. Bayesian model comparison for compartmental models with applications in positron emission tomography. *J. Appl. Stat.* **2013**, *40*, 993–1016.
61. Zhu, W.; Ouyang, J.; Rakvongthai, Y.; Guehl, N.; Wooten, D.; El Fakhri, G.; Normandin, M.; Fan, Y. A Bayesian spatial temporal mixtures approach to kinetic parametric images in dynamic positron emission tomography. *Med. Phys.* **2016**, *43*, 1222–1234.
62. Zuo, Y.; Qi, J.; Wang, G. Relative Patlak plot for dynamic PET parametric imaging without the need for early-time input function. *Phys. Med. Biol.* **2018**, *63*, 165004.